Torque control for a flux-switching permanent-magnet motor based on FEM data

Riccardo Donazzolo

School of Electrical Engineering

Espoo 25.6.2018

Supervisor

Prof. Marko Hinkkanen

Aalto University
School of Electrical
Engineering

Aalto University
School of Electrical
Engineering

Aalto University, P.O. BOX 11000, 00076 AALTO
www.aalto.fi
Abstract of the Final Project

Author Riccardo Donazzolo

Title Torque control for a flux-switching permanent-magnet motor based on FEM data

Degree programme Electrical Power and Energy Engineering

Major Electric Drives **Code of major** ELEC-E8405

Supervisor and advisor Prof. Marko Hinkkanen

Date 25.6.2018 **Number of pages** 53 **Language** English

Abstract

Flux-switching permanent-magnet (FSPM) motors development became important to the manufacturing companies due to their high torque density and robustness. Moreover the control methods for electric motors are in continuous evolution in order to minimize the losses caused by the drives and to optimize the computational costs. In this final project a 2.2-kW FSPM machine is considered. The aim of this project is to estimate the parameters from FEM data and to use them to parametrize the motor and the control system. All these data are first computed with a FEM software. Then a simplified parameterization that neglects the cross-coupling and saturation is used for the control system. Particularly, the collected data are also needed in order to build the look-up tables for the reference calculation, essential for having an efficient control design with a low computational cost. In order to obtain maximum torque taking into account the current and voltage limits, the maximum torque per ampere (MTPA), maximum torque per volt (MTPV) and field weakening (FW) strategies are employed. The final simulation scheme is a control system with a simple parameterization and a plant model which includes saturation and cross-coupling. Hence the error caused by the neglected saturation and the performance of the control system are analyzed.

Keywords current control , discrete-time , finite elements analysis , flux switching permanent magnets , look-up tables , pole placement , torque control

Preface

I want to thank prof. Marko Hinkkanen and the Aalto University for this opportunity, I have learnt much from this experience. This thesis is dedicated to my Family, to Alessia, to "civico 4" members and to the Universities of Padova and Aalto.

Otaniemi, 24.6.2018

Riccardo Donazzolo

Contents

Symbols and abbreviations

Symbols

Boldface letters represent the matrices and the vectors. Reference values are marked by the subscript ref.

$a_{\mathrm{d0}}, a_{\mathrm{q0}}, a_{\mathrm{dd}}, a_{\mathrm{qq}}, a_{\mathrm{dq}}$	saturation model coefficients
A_{z}	vector potential
dq	rotating or synchronous coordinates
$\mathbf{F}_{\mathrm{c}}$	system matrix of continuous-time domain
$\boldsymbol{g}_{\mathrm{c}}$	system matrix
$\mathbf{G}_{\mathrm{c}}$	system matrix of continuous-time domain
$\mathbf{I}$	identity matrix
I	peak current
I_{ch}	characteristic current
i_{f}	constant current corresponding to PMs
$\boldsymbol{i}_{\mathrm{s}}$	stator current real space vector in synchronous coordinates
i_{d}	d-axis component of the stator current
i_{q}	q-axis component of the stator current
$i_{\mathrm{d,ref}}$	reference d-axis component of stator current
$i_{\mathrm{q,ref}}$	reference q-axis component of stator current
I_{rms}	RMS value of current
I_{slot}	total current in the slot
$\mathbf{J}$	orthogonal rotation matrix
J	current density
J_{tot}	total moment of inertia
k	discrete-time index
k_{fill}	fill factor
L_{d}	d-axis inductance
L_{q}	q-axis inductance
L_{ew}	length of end of winding
L_{stk}	length of stack winding
L_{tot}	total length of winding
M	mass of rotor
N	number of phase turns
n_{cs}	number of conductors in slot
$\mathbf{O}$	zero matrix
p	number of pole teeth
P_{j}	total copper losses
Q_{s}	stator slot number
R_{s}	stator resistance
S_{slot}	slot section
S, T, U, V, U', V'	saturation model exponents

T_{em}	electromagnetic torque
T_{s}	sampling period
u_{dc}	DC-link voltage
$\boldsymbol{u}_{\mathrm{s}}$	stator voltage real space vector in synchronous coordinates
u_{d}	d-axis component of the stator voltage
u_{q}	q-axis component of the stator voltage
V_{cu}	total volume of copper
V_{rotor}	volume of the rotor
δ_{k}	duty cycle
ω_{m}	electrical angular speed
$\rho_{120°}$	copper resistivity at 120°
ρ_{iron}	mass density of iron
ψ_{m}	permanent-magnet flux
$\boldsymbol{\psi}_{\mathrm{s}}$	stator flux real space vector in synchronous coordinates
ψ_{d}	d-axis component of the stator flux
ψ_{q}	q-axis component of the stator flux
ξ	saliency ratio

Operators

$\frac{\mathrm{d}}{\mathrm{d}t}$	derivative with respect to variable t

Abbreviations

2DOF	2 degrees of freedom
FEM	finite element method
FSPM	flux-switching permanent-magnet
FW	field weakening
IPM	interior permanent magnets
LLS	linear least squares
MTPA	maximum torque per ampere
MTPV	maximum torque per volt
PI	proportional integral
PM	permanent magnet
PWM	pulse width modulation
SPM	surface-mounted permanent magnets
ZOH	zero order hold

1 Introduction

Flux-switching permanent-magnet (FSPM) is a kind of brushless synchronous machine, of which both permanent magnets and armature windings are located in the stator and the rotor shows a simple salient-pole structure. This kind of machine has been extensively investigated and applied in high performance and critical drive fields due to the remarkable advantages, including high efficiency, robust structure, high power density and torque density. Furthermore the fact that the magnets are buried in the stator makes the temperature easier to control in order to prevent the demagnetization. This motor can be used in a wide range of applications, as electric vehicles, aircraft, fans, pumps, and others industrial machines that need high torque values [13].

Regarding the control drives, continuous researches are done in order to optimize the computation costs and to maximize the performance of the machines. The use of look-up tables turned out to be a method to reach these objectives. The look-up tables link a signal directly to another prefixed one without any additional computation. They can be based both on the FEM data or from the measurement on the real motor. The used control scheme is based on [7],[8], [9], [10], which use a digital discrete-time implementation.

The objective of this final project is to evaluate the performance of a discrete-time control drive that neglects the iron saturation applied to a 2.2-kW FSPM motor. The parameterization of the control system is based on FEM data. The performances are studied through a comparison between the use of two different plant models: one with the same parameterization of the control system and another one that simulates the real behavior of the motor, hence including the saturation.

This final project is divided into six sections. Section 2 details the structure of FSPM motor and motor model in the synchronous rotating reference frame. Section 3 is composed by the estimation of the parameters including MTPA, FW and MTPV computation. ection 4 lists the structure of the used Simulink model. Section 5 shows the simulation results with both the plant models, hence with and without cross saturation. The conclusion based on results are summarized in section 6.

2 Flux-switching permanent-magnet machines

In an interior permanent magnet (IPM) machine, the permanent magnets are buried in the rotor laminations, instead of be mounted on the rotor surface, hence the permanent magnets are well protected from de-magnetization. Further, if the overlapping stator winding is employed, the reluctance torque can be utilized. It is well known that IPM machines exhibit high constant torque capability and excellent constant power capability.

In a flux-switching permanent-magnet (FSPM) machine, the permanent magnets are located on the stator, which makes the temperature rise in the permanent magnets much easier to be controlled. The rotor is very simple and robust, so that it can be operated at very high speed. Furthermore the main characteristic of a flux-switching machine is the high torque density, making it a very good machine type.

The flux switching is obtained thanks to the double salience (both on stator and rotor) and to the rotor rotation. The first flux switching machine has been presented in 1955 from the US engineers S.E. Rauch and L.J. Johnson as a mono-phase alternator version [3].

2.1 Working principle

In order to explain the working principle of a flux-switching machine, Fig. 1 is taken as a reference. In the example, the rotor is represented as a stack of laminations with two salient poles, while the stator is made up of a couple of permanent magnets, a dual set of laminated jokes and a pair of windings.

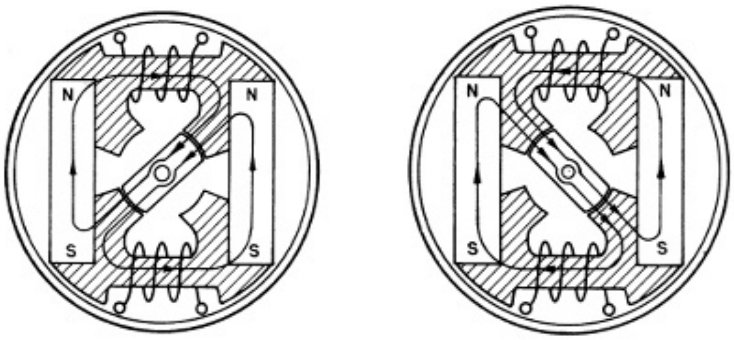

(a) (b)

Figure 1: Flux-switching alternator, [3]: position 0°(a) and position 180°(b)

The flux paths in Fig. 1 (a) are directed from left to right in both the windings. When the rotor is rotated of 90°(180 electrical degrees), as shown in Fig. 1 (b), the flux linkage has the opposite direction, but the peak value is the same as in the first

case. This means that every 360 mechanical degrees four complete flux switchings are obtained, hence two periods of its waveform.

In order to have a flux path with a constant reluctance, which aims to reduce the eddy currents and with them the losses, the number of rotor poles must be higher than the number of stator poles.

Furthermore the back EMF in the windings is ideally sinusoidal, which means that the use of traditional dq control method is possible.

The advantages of such type of machine are:

- Robustness, due to the fact that PMs are located into the stator, so the rotor is solely made of laminated iron.
- High torque density, which means that compared to other machine types with the same size, the FSPM machine has higher torque values.
- Easiness on controlling the magnets temperature.
- Sinusoidal back-EMF

while the disadvantages are:

- Building difficulties, due to the PMs inside of the stator core.
- Knowing that the electrical angular speed is $\omega_{\mathrm{m}} = p\omega$, where ω is the mechanical speed and p is the number of rotor teeth, it can be noticed that an high number of teeth on the rotor implies a high fundamental frequency. Therefore an high switching frequency on the converter is needed.

2.2 Model of the motor

The general laws that describe the voltage and the torque of a synchronous motor are [11]:

$$\begin{cases} u_{\mathrm{d}} = \frac{d\psi_{\mathrm{d}}}{dt} - \omega_{\mathrm{m}}\psi_{\mathrm{q}} + R_{\mathrm{s}} i_{\mathrm{d}} \\ \\ u_{\mathrm{q}} = \frac{d\psi_{\mathrm{q}}}{dt} + \omega_{\mathrm{m}}\psi_{\mathrm{d}} + R_{\mathrm{s}} i_{\mathrm{q}} \end{cases} \tag{1}$$

$$T_{\mathrm{em}} = \frac{3}{2} p(\psi_{\mathrm{d}} i_{\mathrm{q}} - \psi_{\mathrm{q}} i_{\mathrm{d}}) \tag{2}$$

The flux-switching PM machine can be studied, for control purpose, as an IPM machine due to the anisotropy between the d-axis and q-axis.

The ideal mathematical model in dq coordinates, where d-axis and q-axis are decoupled, can be given as:

$$\begin{cases} \psi_{\mathrm{d}} = \psi_{\mathrm{m}} + L_{\mathrm{d}} i_{\mathrm{d}} \\ \psi_{\mathrm{q}} = L_{\mathrm{q}} i_{\mathrm{q}} \end{cases} \tag{3}$$

$$T_{\mathrm{em}} = \frac{3}{2} p[\psi_{\mathrm{m}} i_{\mathrm{q}} + (L_{\mathrm{d}} - L_{\mathrm{q}}) i_{\mathrm{d}} i_{\mathrm{q}}] \tag{4}$$

where ψ_{d} and ψ_{q} are d-axis and q-axis flux linkage, L_{d} and L_{q} are d-axis and q-axis inductances, u_d and u_q are d-axis and q-axis voltage, ψ_{m} is amplitude of phase flux linkage produced by permanent magnet, ω_{m} is electrical angular speed, R_{s} is resistance of phase winding and p is the number of poles.

Furthermore equations (3) are no more valid if the cross-coupling is taken into account and the flux linkages are generally functions of both the currents

$$\psi_{\mathrm{d}} = \psi_{\mathrm{d}}(i_{\mathrm{d}}, i_{\mathrm{q}}), \qquad \psi_{\mathrm{q}} = \psi_{\mathrm{q}}(i_{\mathrm{d}}, i_{\mathrm{q}}) \tag{5}$$

The three-phase currents referred to the dq coordinates system are calculated using the Park transformation.

From the abc to dq coordinates system the relations are:

$$\begin{aligned} i_{\mathrm{d}} &= \frac{2}{3}[i_{\mathrm{a}} \cos(\theta_{\mathrm{m}}) + i_{\mathrm{b}} \cos(\theta_{\mathrm{m}} - \frac{2}{3}\pi) + i_{\mathrm{c}} \cos(\theta_{\mathrm{m}} + \frac{2}{3}\pi)] \\ i_{\mathrm{q}} &= \frac{2}{3}[-i_{\mathrm{a}} \cos(\theta_{\mathrm{m}}) - i_{\mathrm{b}} \cos(\theta_{\mathrm{m}} - \frac{2}{3}\pi) - i_{\mathrm{c}} \cos(\theta_{\mathrm{m}} + \frac{2}{3}\pi)] \end{aligned} \tag{6}$$

and vice versa:

$$\begin{aligned} i_{\mathrm{a}} &= i_{\mathrm{d}} \cos(\theta_{\mathrm{m}}) - i_{\mathrm{q}} \sin(\theta_{\mathrm{m}}) \\ i_{\mathrm{b}} &= i_{\mathrm{d}} \cos(\theta_{\mathrm{m}} - \frac{2}{3}\pi) - i_{\mathrm{q}} \sin(\theta_{\mathrm{m}} - \frac{2}{3}\pi) \\ i_{\mathrm{c}} &= i_{\mathrm{d}} \cos(\theta_{\mathrm{m}} + \frac{2}{3}\pi) - i_{\mathrm{q}} \sin(\theta_{\mathrm{m}} + \frac{2}{3}\pi) \end{aligned} \tag{7}$$

Equations (6) and (7) can be also used to transform the fluxes and the voltages.

3 Estimation of the motor parameters

The FSPM motor geometry is shown in Fig. 2 while the winding scheme is shown in Fig. 3. Furthermore the used materials are shown in Table 1. The motor that is considered in this final project has been designed in [1], [2].

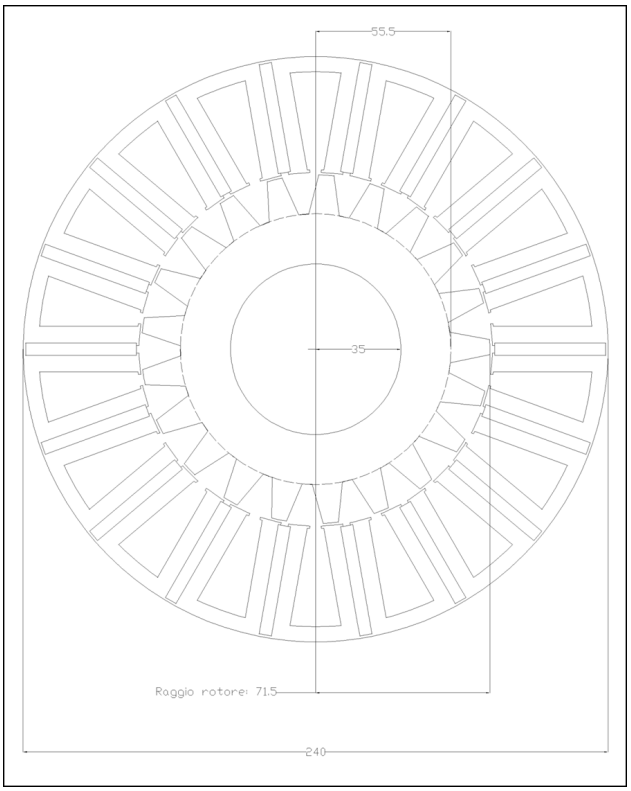

Figure 2: FSPM motor geometry [mm]

Machine component	Material
Stator	Laminated iron
Rotor	Laminated iron
Phase windings	Copper Cu10
Shaft	Stainless steel
Permanent magnets	NdFeB

Table 1: Machine materials

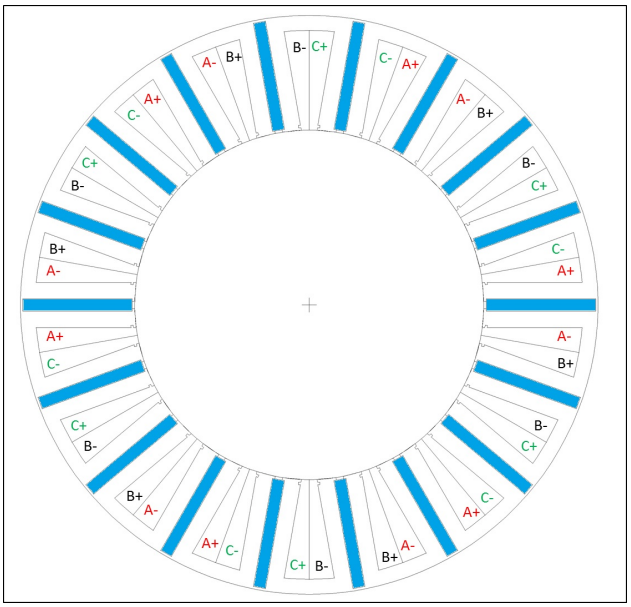

Figure 3: Winding scheme

3.1 Main data of the machine

The main data of the machine are reported in the following tables. Table 2 gives the nominal data of the FSPM motor. In Table 3 the main stator geometrical data are listed, and in Table 4 the winding data are reported.

Parameter	Value
Nominal voltage [V]	720
Nominal current [A]	3.74
Nominal frequency [Hz]	50
Nominal torque [Nm]	148.5
Rotor teeth	21
Stator teeth	18

Table 2: Machine nominal data

Parameter	Value
Stator package length [mm]	120
External stator diameter [mm]	240
Stator slot number	18
Slot cross section area [mm^2]	561
External rotor diameter [mm]	143
Shaft diameter [mm]	70

Table 3: Stator parameters

Parameter	Value
Stack length [mm]	120
End winding length [mm]	41.6
Number of conductors, n_{cs}	360
Single wire section [mm^2]	0.62

Table 4: Winding data

3.2 Stator current

It is important to estimate the maximum current permissible in the stator winding. Knowing the geometry of the motor from [1], [2], using the slot cross-section area

$$S_{\text{slot}} = 561\,\text{mm}^2,$$

assuming a current density:

$$J = 6\,\text{A/mm}^2$$

and a fill factor of the slot:

$$k_{\text{fill}} = 0.4$$

the total current in the slot is equal to:

$$I_{\text{slot}} = \sqrt{2} \cdot J \cdot S_{\text{slot}} \cdot k_{\text{fill}} = 1904\,\text{A}$$

The maximum peak current in each phase conductor should be less than:

$$I = \frac{I_{\text{slot}}}{n_{\text{cs}}} = 5.29\,\text{A}$$

The RMS value of the current is:

$$I_{\mathrm{rms}} = \frac{I}{\sqrt{2}} = 3.74\,\mathrm{A}$$

3.3 Winding

According to the stator slot number $Q_{\mathrm{s}} = 18$ the slot angle results in:

$$\alpha_{\mathrm{s}} = \frac{360}{18} = 20°$$

For automatic computation and current setting in the stator slot, a slot matrix is implemented. This is constructed using a $+0.5$ where the current is going out and -0.5 where the current is entering. The FSPM motor has 18 stator slots and 6 phase poles, hence the slot matrix exhibits a periodicity. Table 5 reports the matrix used for this motor.

slot (q)	1	2	3	4	5	6	7	8	9	10	11	12	13	14	15	16	17	18
k_{a}	$\frac{1}{2}$	0	$-\frac{1}{2}$	$\frac{1}{2}$	0	$-\frac{1}{2}$	$\frac{1}{2}$	0	$-\frac{1}{2}$	$\frac{1}{2}$	0	$-\frac{1}{2}$	$\frac{1}{2}$	0	$-\frac{1}{2}$	$\frac{1}{2}$	0	$-\frac{1}{2}$
k_{b}	0	$-\frac{1}{2}$	$\frac{1}{2}$	0	$-\frac{1}{2}$	$\frac{1}{2}$	0	$-\frac{1}{2}$	$\frac{1}{2}$	0	$-\frac{1}{2}$	$\frac{1}{2}$	0	$-\frac{1}{2}$	$\frac{1}{2}$	0	$-\frac{1}{2}$	$\frac{1}{2}$
k_{c}	$-\frac{1}{2}$	$\frac{1}{2}$	0	$-\frac{1}{2}$	$\frac{1}{2}$	0	$-\frac{1}{2}$	$\frac{1}{2}$	0	$-\frac{1}{2}$	$\frac{1}{2}$	0	$-\frac{1}{2}$	$\frac{1}{2}$	0	$-\frac{1}{2}$	$\frac{1}{2}$	0

Table 5: Stator slot Matrix

k_{a}, k_{b}, k_{c} are respectively the slot matrices of phase a, b and c. These matrices are necessary to automatically compute the flux linkages. The absolute value of the matrix elements specifies the relative filling of the q-th slot by the interested phase [12]. The fact that the absolute value is 0.5 implies that a single slot is filled with two different phases as shown in Fig. 3.

3.4 Phase resistance

The stator winding material is copper, therefore the used value of resistivity is

$$\rho_{120°} = 0.023 \cdot 10^{-6}\,\Omega\mathrm{m}$$

where the reference temperature is for assumption 120°[1],[2]. For computing the stator resistance, it is necessary to know the total length of the conductor:

$$L_{\mathrm{tot}} = L_{\mathrm{stk}} + L_{\mathrm{ew}} = 120\,\mathrm{mm} + 41.6\,\mathrm{mm} = 161.6\,\mathrm{mm}$$

so the total stator winding resistance can be obtained by:

$$R_\mathrm{s} = 2 \cdot \rho_{120^\circ} \cdot \frac{N \cdot L_\mathrm{tot}}{S_\mathrm{c}} = 12.98\,\Omega$$

where N is total number of phase turns, S_c is cross-section area of the conductors, which is $0.62\,\mathrm{mm}^2$.

Another possible way to estimate the phase resistance is to use the losses in the entire winding. The result has to be the same. The copper losses are [1],[2]

$$P_\mathrm{j} = \rho_{120} \cdot J^2 \cdot V_\mathrm{cu} = 541\,\mathrm{W} \tag{8}$$

where:

- $\rho_{120^\circ} = 0.023 \cdot 10^{-6}\,\Omega m$
- $V_\mathrm{cu} = N_\mathrm{s} \cdot k_\mathrm{fill} \cdot (L_\mathrm{stk} + L_\mathrm{ew}) = 18 \cdot 0.4 \cdot 561 \cdot 10^{-6} \cdot (120 + 41.6) \cdot 10^{-3} = 6.53 \cdot 10^{-4}\,\mathrm{m}^3$
- $J = 6\,\mathrm{A/mm}^2$

Phase resistance can be expressed as:

$$R_\mathrm{s} = \frac{2}{3}\frac{P_\mathrm{j}}{I^2} = 12.89\,\Omega$$

3.5 Permanent magnet flux linkage

For the computation of the PM flux a MATLAB script is used to evaluate the flux linkage varying the position of the rotor without phase currents from the FE model. The computation is made between 0°and 17.14°, which is the electrical period of the machine. The used script does the following operations:

1. Set the phase currents to 0, which are given through the Park transformation in (7) while $i_\mathrm{d} = 0$ and $i_\mathrm{q} = 0$ is given.
2. Solve the magnetic problem;
3. Compute the flux linkages using the slot matrix (Tab. 5) and integrating the vector potential A_z over the stator slot surfaces, as:

$$\psi_\mathrm{a} = L_\mathrm{stk} \sum_{q=1}^{Q_\mathrm{s}} n_\mathrm{aq} \frac{1}{S_\mathrm{slot}} \int_{S_\mathrm{slot}} A_\mathrm{z}\, dS$$

$$\psi_\mathrm{b} = L_\mathrm{stk} \sum_{q=1}^{Q_\mathrm{s}} n_\mathrm{bq} \frac{1}{S_\mathrm{slot}} \int_{S_\mathrm{slot}} A_\mathrm{z}\, dS$$

$$\psi_\mathrm{c} = L_\mathrm{stk} \sum_{q=1}^{Q_\mathrm{s}} n_\mathrm{cq} \frac{1}{S_\mathrm{slot}} \int_{S_\mathrm{slot}} A_\mathrm{z}\, dS$$

where L_{stk} is the stack length of the motor, S_{slot} is the cross–section area of the slot, and n_{aq}, n_{bq}, and n_{cq} are the numbers of series conductors of the phase a, b, and c within the q–th slot of the stator.

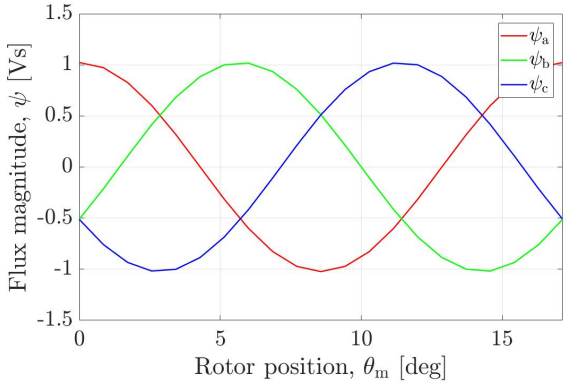

Figure 4: No load flux linkages

It can be seen from Fig. 4 that the flux linkage has a sinusoidal form and the peak value is 1.023 Vs.

3.6 Moment of inertia

Since the geometry of the machine is known, it is possible to estimate the moment of inertia, J_{tot}, of the rotor. It is assumed that:

- the rotor is made entirely by laminated iron, since the difference between iron and steel densities can be neglected. Hence the assumed mass density is

$$\rho_{\text{iron}} = 7.874\,\text{g/cm}^3$$

- The rotor is a cylinder with radius $r = 7.15\,[\text{cm}]$ and height $H = 12\,\text{cm}$

After these assumptions it is easy to estimate the moment of inertia through the equation

$$J_{\text{tot}} = \frac{1}{2}Mr^2 = 3.88 \cdot 10^{-2}\,\text{kgm}^2$$

where M is the rotor mass, which is computed as follows

$$M = \rho_{iron}V_{\text{rotor}} = \rho_{\text{iron}}\pi r^2 H = 15.175\,\text{kg}$$

Moreover, in order to take into account something connected to the shaft, J_{tot} will be multiplied by 10 for the simulations.

3.7 Operating points

The operating points will be computed using the FEM data, then a couple of fixed inductances will be chosen in order to simplify the control model.

Loci with variable inductances

It is important to notice that these computations were done with the FEM model in a static simulation, moreover to compute these values the following approximations were used

$$I_{\mathrm{ch}} = -\frac{\psi_{\mathrm{m}}}{L_{\mathrm{d}}} \tag{9}$$

where I_{ch} is the characteristic current, ψ_{m} is the permanent magnet flux and L_{d} is the direct inductance computed in every point with the following relation:

$$L_{\mathrm{d}} = \frac{\psi_{\mathrm{d}} - \psi_{\mathrm{m}}}{i_{\mathrm{d}}} \tag{10}$$

It is evident that this approach leads to an error given by the saturation. Moreover, for the current limit and MTPV loci computation, the machine was considered as a SPM machine. This can be done because the torque map in the interested dq function region presents flat torque curves in the dq plane which are a characteristic of such type of machine (Fig. 5).

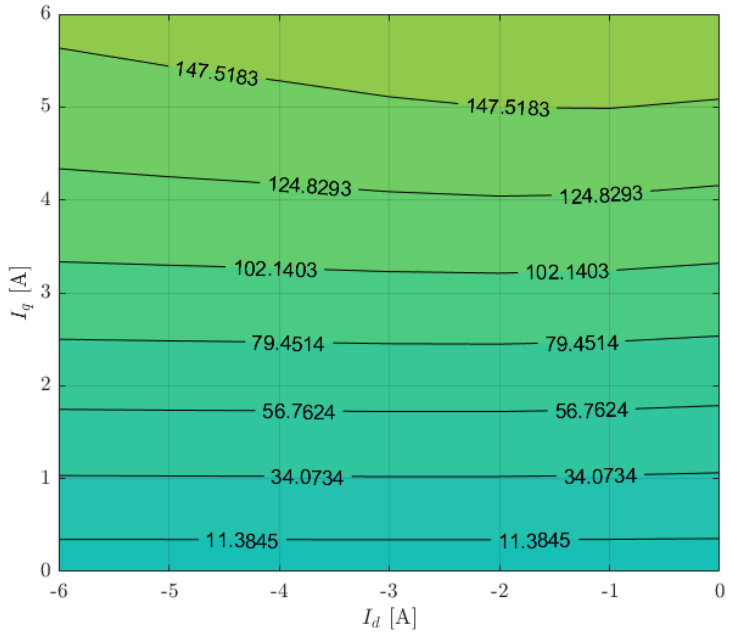

Figure 5: Torque map in the second quadrant, the values refer to a given dq current and are expressed in Nm

- MTPA locus

  In order to compute the MTPA (maximum torque per ampere) locus, a script was used in which a range of current peak and a range of current angles are the inputs. Then the torque will be evaluated and, for every current peak value, the angle that gives the maximum torque is computed.

  The given maximum torques for every angles are shown in Fig. 6.

  Using these data, it is possible to draw the MTPA current locus in the dq plane (Fig. 7).

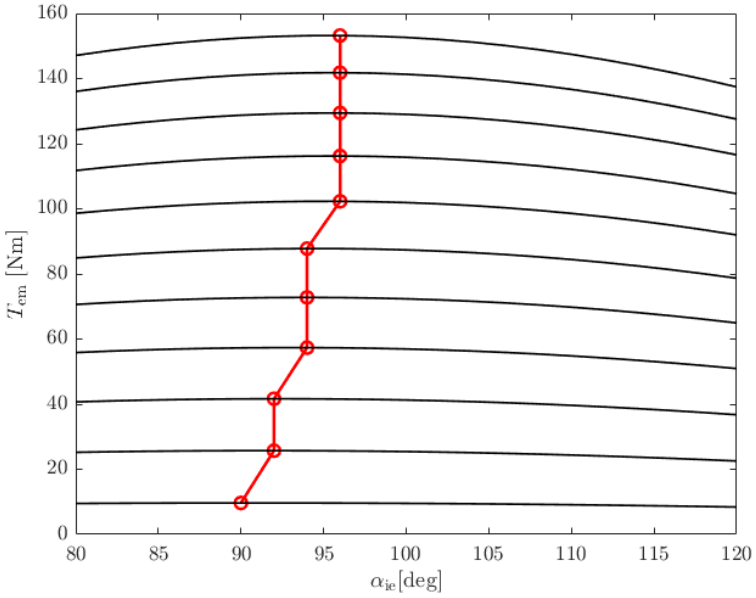

Figure 6: Given torque and *dq* current phase varying the current peak and current angle

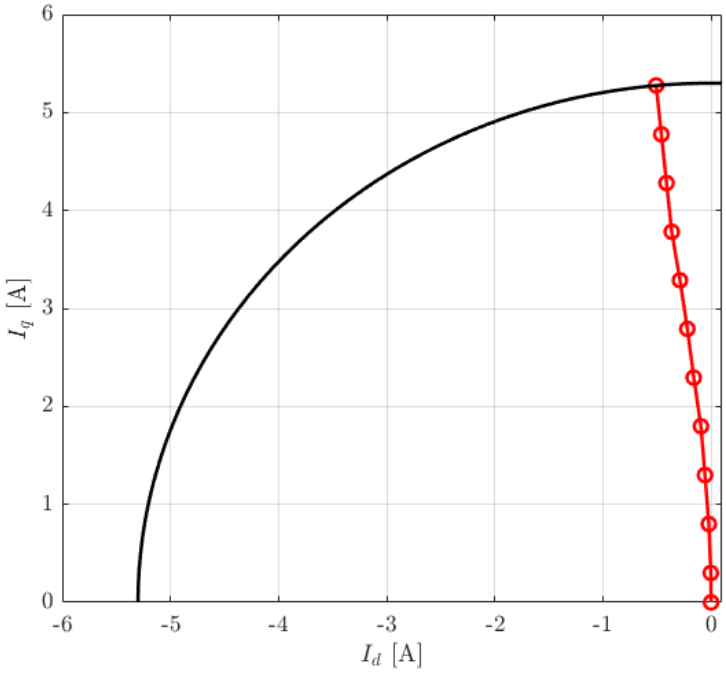

Figure 7: MTPA current locus

Moreover, in every evaluated point, fluxes and torque were computed in order to build the desired look-up tables.

- Current Limit locus

  For the current limit locus the starting point was given as input, which is the last one of the MTPA locus and, varying the current phase with the current peak fixed to the rated value, the characteristic current is evaluated for every point. This iteration is done with an if-cycle in which the direct current must be smaller than the characteristic one.

  In the following plot the resulting locus and the computed characteristic currents are given.

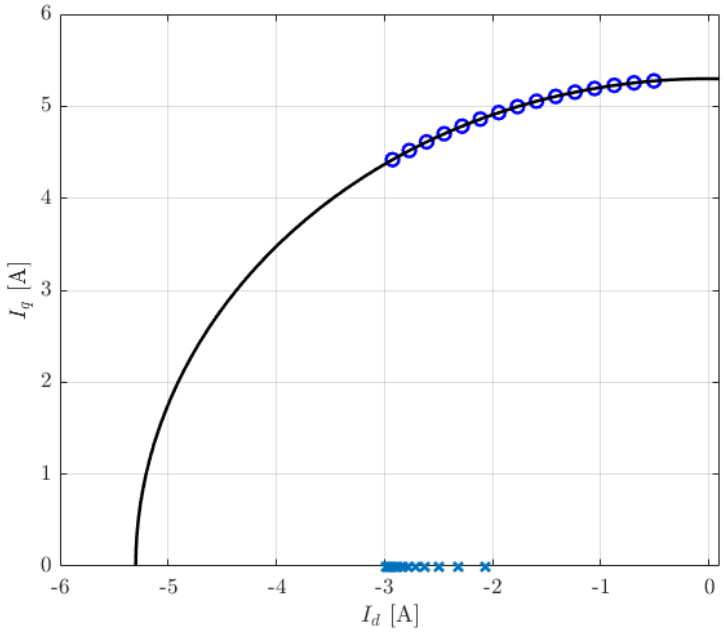

Figure 8: Current limit locus

- MTPV locus

  In a similar way to the current limit locus, the MTPV (maximum torque per voltage) locus is computed and the resulting plot is shown in Fig. 9.

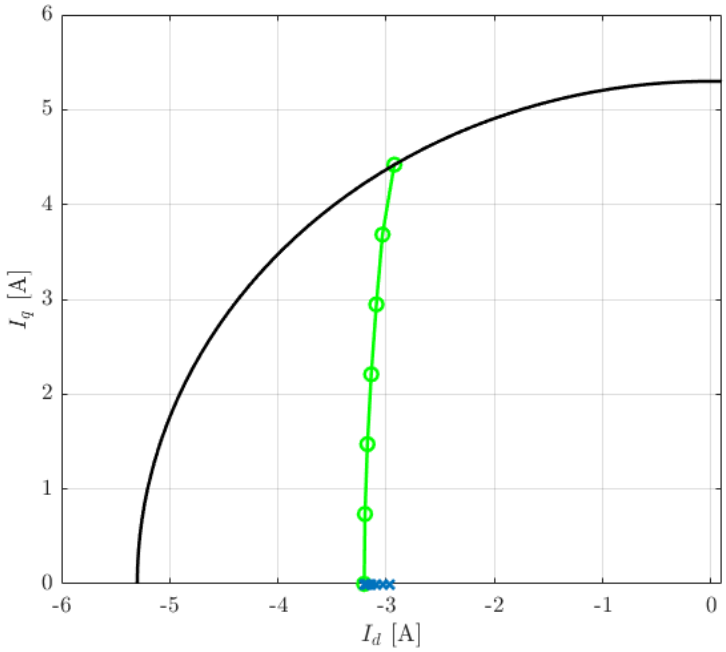

Figure 9: MTPV current locus

In Fig. 10 the loci are plotted together.

In Figures 8 and 9 it is important to notice that the variation of the inductances leads to the variation of I_{ch}, i.e. in the first locus the characteristic current varies from -2 to $-3\,\mathrm{A}$, while in the second one it reaches the value of $-3.3\,\mathrm{A}$.

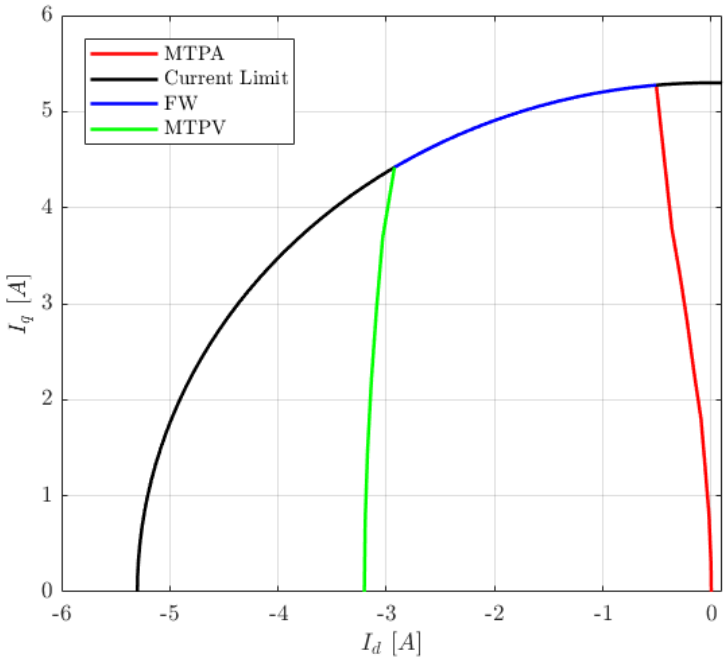

Figure 10: Maximum torque loci

Loci with fixed inductances

In the previous computations equation (3) was used in order to find the values of the inductances at every operating point. Then using equations (3) and (4) with fixed inductances the current loci has been found. In order to find a feasible choice of inductances the following operating points were taken as samples:

Locus	i_d [A]	i_q [A]	L_d [H]	L_q [H]
MTPA	-0.5080	5.2756	0.4962	0.2975
FW	-0.8748	5.2273	0.3899	0.3022
MTPV	-3.1383	2.2098	0.3283	0.3333

The previous table shows that the saliency ratio, which is

$$\xi = \frac{L_\mathrm{d}}{L_\mathrm{q}}$$

varies over the different operating points. Moreover it is important to notice that the ratio is not always under the unity, which would be a characteristic of standard IPM machines.

This would lead to a MTPA locus located in the first quadrant with $i_\mathrm{d} > 0$. The resulting ideal loci for the chosen inductances are shown in Fig 11.

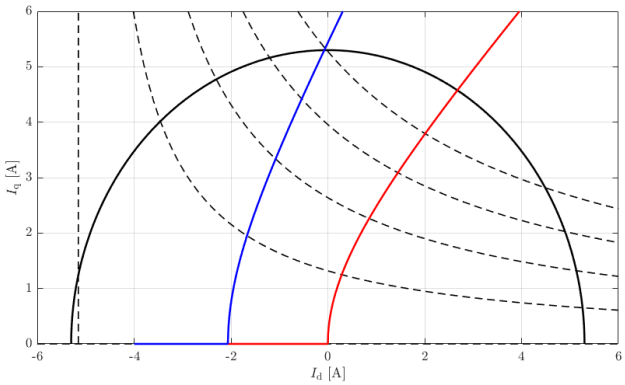

(a) $L_\mathrm{d} = 0.4962\,\mathrm{H} \quad L_\mathrm{q} = 0.2975\,\mathrm{H}$

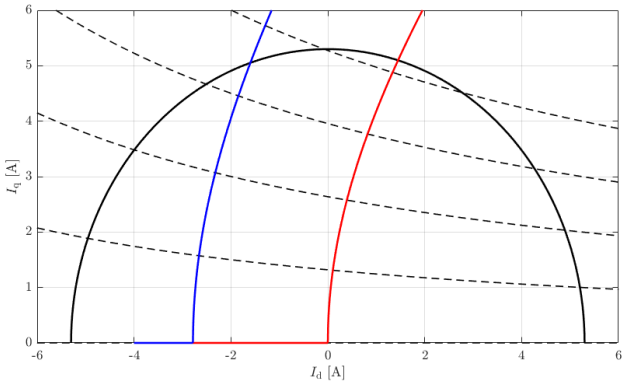

(b) $L_\mathrm{d} = 0.3899\,\mathrm{H} \quad L_\mathrm{q} = 0.3022\,\mathrm{H}$

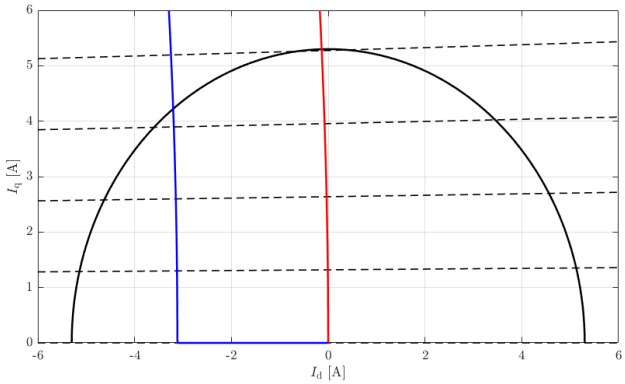

(c) $L_\mathrm{d} = 0.3283\,\mathrm{H} \quad L_\mathrm{q} = 0.3333\,\mathrm{H}$

Figure 11: MTPA/MTPV loci varying the inductances values

From the computation of MTPA based on the FEM data, a locus in the first quadrant is not expected, so the most reasonable choice is the locus in Fig. 11(c) which is similar to the one in Fig. 10.

These results lead to the following choice of inductances:

$$L_\mathrm{d} = 0.3283\,\mathrm{H}$$
$$L_\mathrm{q} = 0.3333\,\mathrm{H} \tag{11}$$

It is remarkable that the rated torque computed with fixed inductances is higher than the one obtained with FEMM, which is computed with

$$T_\mathrm{em} = \frac{3}{2} p(\psi_\mathrm{d} i_\mathrm{q} - \psi_\mathrm{q} i_\mathrm{d})$$

where the values of the dq fluxes are computed with the software. The rated torque given from FEM is equal to 153 Nm while the one calculated with fixed inductances is 170 Nm, this leads to an error equal to ≈11% of the real value (Tab. 2). This error is clearly caused by the iron saturation.

In Fig. 12 the comparison between the two kinds of loci is shown.

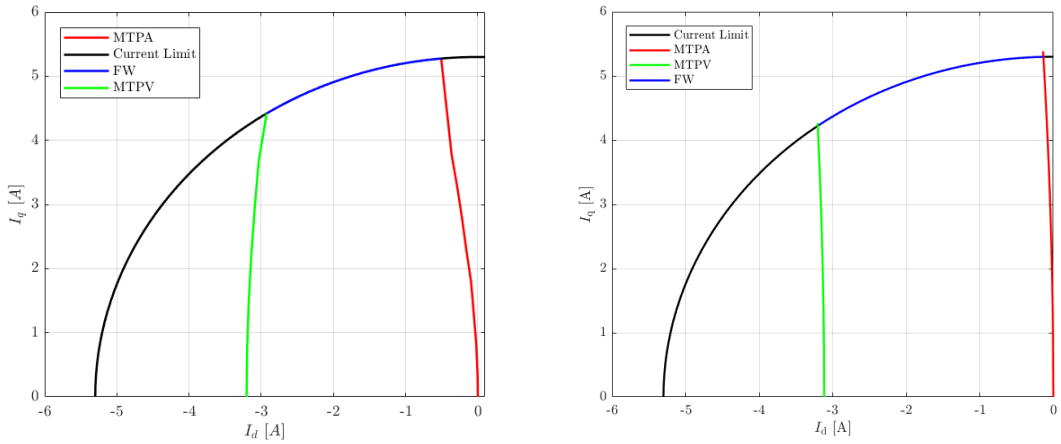

(a) Loci computed from FEM data

(b) Loci computed with fixed inductances

Figure 12: Comparison between the loci based on FEM data and the ones based on fixed inductances

The approach used for (b) presents obviously an error in the computation of the operating points.

4 Simulink model

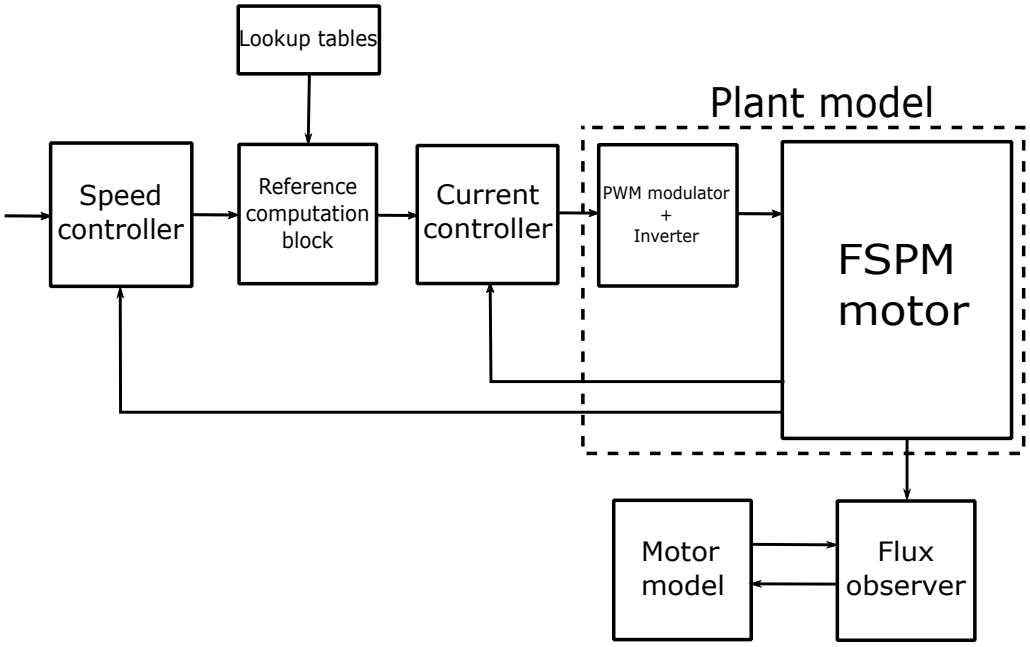

Figure 13: Control model

The used control model is shown in Fig. 13 and its components will be explained in this chapter.

4.1 Plant model

Motor model

In a first approximation, the motor could be modeled neglecting the saturation and the equations (3) could be used. Hence, we could use fixed inductances L_d and L_q modeling the fluxes as linear functions of currents as we did previously in figures 11, so using the values in (11).

To get a sufficiently realistic model of the motor, the software FEMM is used to compute the fluxes as function of dq currents. This is needed in order to build an algebraic magnetic model with the LLS (linear least squares) method. This method purpose is to find a polynomial characteristic which fits with the provided data. In this case the input data will be the flux mapping computed from the FE analysis, and the results will be $i_\mathrm{d}(\psi_\mathrm{d}, \psi_\mathrm{q})$ and $i_\mathrm{q}(\psi_\mathrm{d}, \psi_\mathrm{q})$. The method used to map the fluxes is similar to the one used for the computation of the permanent magnet flux linkage in section 3.5, but the rotor is fixed on the α-axis and the currents vary at every iteration in order to build a matrix in which the indices represent the dq currents.

The obtained *dq* axis flux maps are shown in Fig. 14.

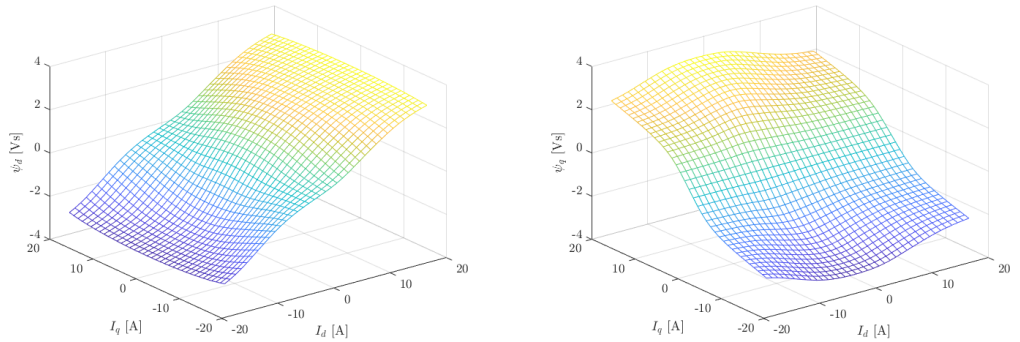

(a) *Flux on d-axis* (b) *Flux on q-axis*

Figure 14: d-q axis Flux

The current components

$$i_\mathrm{d} = i_\mathrm{d}(\psi_\mathrm{d}, \psi_\mathrm{q}), \qquad i_\mathrm{q} = i_\mathrm{q}(\psi_\mathrm{d}, \psi_\mathrm{q}) \tag{12}$$

are generally nonlinear function of flux components due to the effect of saturation.

The use of a suitable algebraic magnetic model for (12) makes the number of the parameters to be identified reduced.

For modeling the characteristics (12) with the effect of cross-saturation the following form is applied

$$i_\mathrm{d}(\psi_\mathrm{d}, \psi_\mathrm{q}) = i_\mathrm{d}(\psi_\mathrm{d}, 0) + a'_\mathrm{dq}|\psi_\mathrm{d}|^U|\psi_\mathrm{q}|^{V'}\psi_\mathrm{d} - i_\mathrm{f} \tag{13a}$$
$$i_\mathrm{q}(\psi_\mathrm{d}, \psi_\mathrm{q}) = i_\mathrm{q}(0, \psi_\mathrm{q}) + a'_\mathrm{qd}|\psi_\mathrm{d}|^{U'}|\psi_\mathrm{q}|^V\psi_\mathrm{q} \tag{13b}$$

where a'_dq and a'_qd are nonnegative coefficients, U, U', V, and V' are nonnegative exponents, i_f models the magnetomotive force due to the permanent magnets and

$$i_\mathrm{d}(\psi_\mathrm{d}, 0) = (a_\mathrm{d0} + a_\mathrm{dd}|\psi_\mathrm{d}|^S)\psi_\mathrm{d}$$
$$i_\mathrm{q}(0, \psi_\mathrm{q}) = (a_\mathrm{q0} + a_\mathrm{qq}|\psi_\mathrm{q}|^T)\psi_\mathrm{q}$$

describe the self-axis saturation characteristics.

When taking the reciprocity condition

$$\frac{\partial i_\mathrm{d}(\psi_\mathrm{d}, \psi_\mathrm{q})}{\partial \psi_\mathrm{q}} = \frac{\partial i_\mathrm{q}(\psi_\mathrm{d}, \psi_\mathrm{q})}{\partial \psi_\mathrm{d}}$$

into account, the algebraic model (13) reduces to

$$i_{\mathrm{d}}(\psi_{\mathrm{d}},\psi_{\mathrm{q}}) = (a_{\mathrm{d0}} + a_{\mathrm{dd}}|\psi_{\mathrm{d}}|^{S} + \frac{a_{\mathrm{dq}}}{V+2}|\psi_{\mathrm{d}}|^{U}|\psi_{\mathrm{q}}|^{V+2})\psi_{\mathrm{d}} - i_{\mathrm{f}} \tag{14a}$$

$$i_{\mathrm{q}}(\psi_{\mathrm{d}},\psi_{\mathrm{q}}) = (a_{\mathrm{q0}} + a_{\mathrm{qq}}|\psi_{\mathrm{q}}|^{T} + \frac{a_{\mathrm{dq}}}{U+2}|\psi_{\mathrm{d}}|^{U+2}|\psi_{\mathrm{q}}|^{V})\psi_{\mathrm{q}} \tag{14b}$$

where a_{d0}, a_{dd}, a_{q0}, a_{q0} and a_{dq} are non-negative coefficients, and S, T, U, and V are non-negative exponents. The constant i_{f} models the magnetomotive force due to the permanent magnets. The obtained functions are monotonic and (numerically) invertible, which make them convenient to use.

Using fixed inductances, the equation (14) would reduce to

$$\begin{aligned} i_{\mathrm{d}}(\psi_{\mathrm{d}}) &= a_{\mathrm{d0}}\psi_{\mathrm{d}} - i_{\mathrm{f}} \\ i_{\mathrm{q}}(\psi_{\mathrm{q}}) &= a_{\mathrm{q0}}\psi_{\mathrm{q}} \end{aligned} \tag{15}$$

where

$$\begin{aligned} a_{\mathrm{d0}} &= \frac{1}{L_{\mathrm{d}}} = 3.046\,\mathrm{H}^{-1} \\ a_{\mathrm{q0}} &= \frac{1}{L_{\mathrm{q}}} = 3.001\,\mathrm{H}^{-1} \\ i_{\mathrm{f}} &= \frac{\psi_{\mathrm{m}}}{L_{\mathrm{d}}} = 3.116\,\mathrm{A} \end{aligned}$$

In case that cross-coupling and saturation are taken into account the coefficients a_{dd}, a_{qq}, a_{dq} are non-negative and with the following choice of exponents the resulting currents are given in figure 16, while the fluxes given from the estimated currents is given in figure 15, compared to the one computed from FEM.

S	T	U	V	a_{d0}	a_{dd}	a_{q0}	a_{qq}	a_{dq}	i_{f}
3	4	0	2	2.683	0.104	2.998	0.018	0.184	2.006

Table 6: Fitted parameters for 18-21 FSPM motor

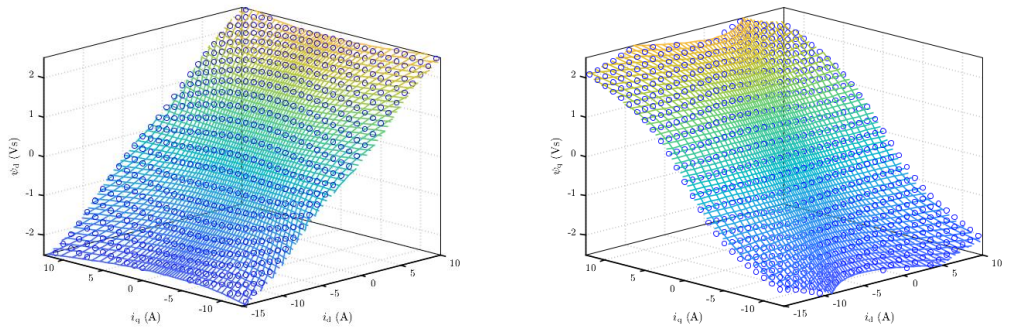

(a) $\psi_\mathrm{d}(i_\mathrm{d}, i_\mathrm{q})$ (b) $\psi_\mathrm{q}(i_\mathrm{d}, i_\mathrm{q})$

Figure 15: Fluxes ψ_dq as function of estimated currents i_dq

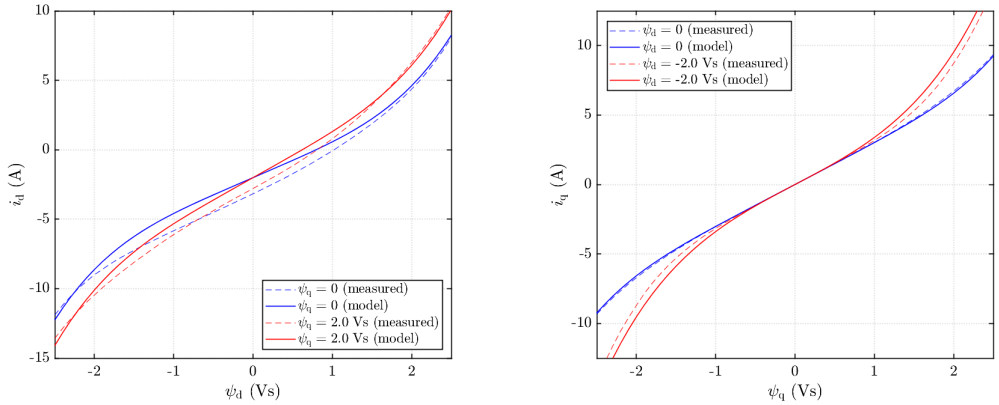

(a) $i_\mathrm{d}(\psi_\mathrm{d})$ (b) $i_\mathrm{q}(\psi_\mathrm{q})$

Figure 16: Currents i_dq as function of fluxes ψ_dq from LLS method

From fig. 16 it can be noticed that the fitted model presents an error, particularly noticeable in Fig. (a). This error is probably caused by the fact that the magnetic model is not suitable enough for this motor. In order to prevent this error in the model, a change in the mathematical model is needed, which is the introduction of a parameter added to ψ_d, which is noted as ψ_F.

The equations in (14) become:

$$i_\mathrm{d}(\psi_\mathrm{d}, \psi_\mathrm{q}) = (a_{\mathrm{d}0} + a_\mathrm{dd}|\psi_\mathrm{d} + \psi_\mathrm{F}|^S + \frac{a_\mathrm{dq}}{V+2}|\psi_\mathrm{d} + \psi_\mathrm{F}|^U|\psi_\mathrm{q}|^{V+2})(\psi_\mathrm{d} + \psi_\mathrm{F}) - i_\mathrm{f} \quad (16a)$$

$$i_\mathrm{q}(\psi_\mathrm{d}, \psi_\mathrm{q}) = (a_{\mathrm{q}0} + a_\mathrm{qq}|\psi_\mathrm{q}|^T + \frac{a_\mathrm{dq}}{U+2}|\psi_\mathrm{d} + \psi_\mathrm{F}|^{U+2}|\psi_\mathrm{q}|^V)\psi_\mathrm{q} \quad (16b)$$

where $\psi_\mathrm{F} = 0.22\,\mathrm{Vs}$ is constant. The LLS method with this added parameters gives the following results:

S	T	U	V	a_{d0}	a_{dd}	a_{q0}	a_{qq}	a_{dq}	i_f
3	4	0	2	2.683	0.087	3.022	0.018	0.176	3.698

Table 7: Fitted parameters for 18-21 FSPM motor with parameter ψ_F

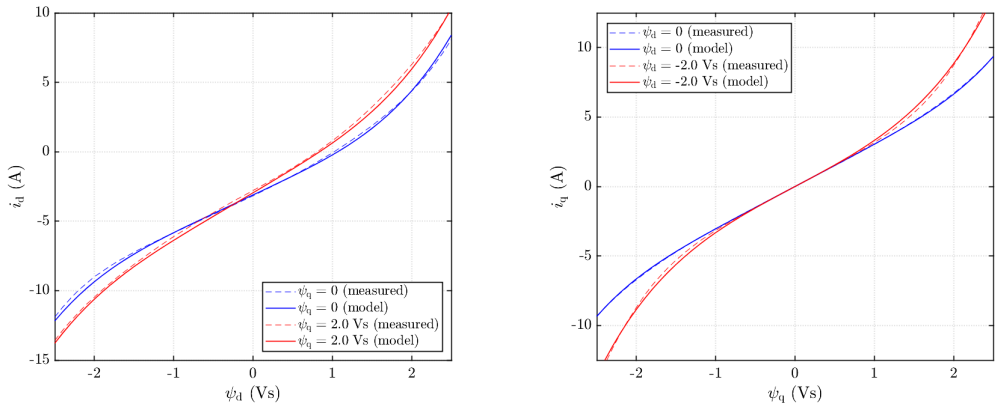

(a) $i_d(\psi_d)$ (b) $i_q(\psi_q)$

Figure 17: Currents i_{dq} as function of fluxes ψ_{dq} from LLS method with ψ_F

Moreover the LLS method gives as feedback the residual statistics in Table 8. The coefficient of determination describes the accuracy of the method. The given results are near to unity, which means that the model fits well with the given data. In both the parameterizations the residual statistics are good, but it is evident, also referring to Figure 17, that the model with ψ_F fits better with the data computed with the FEM simulations.

Residual parameter	without ψ_F	with ψ_F
RMS of residuals [A]	0.546	0.317
Maximum residual [A]	1.316	1.301
Coefficient of determination	0.997	0.999

Table 8: Residual statistics

The used Simulink motor model is the following:

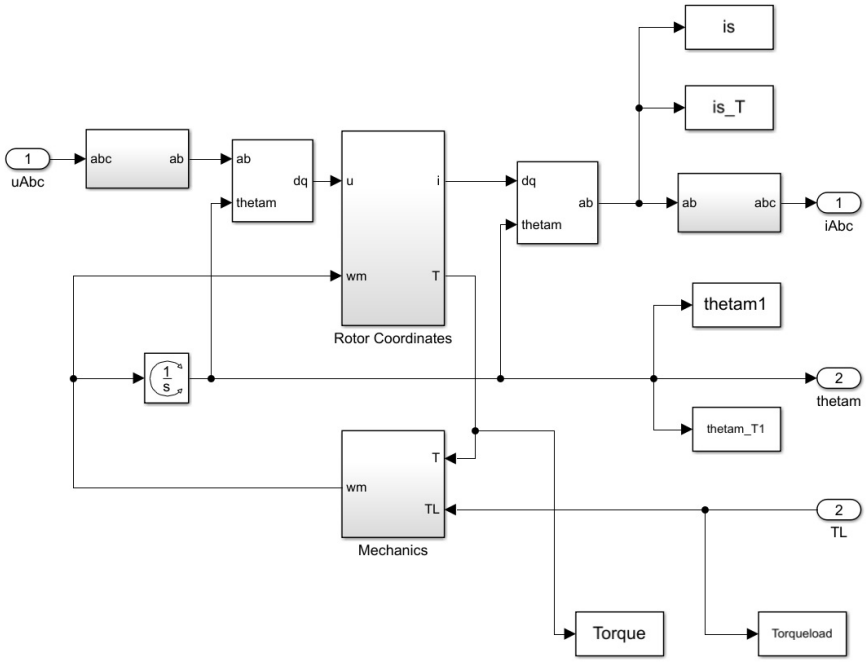

Figure 18: Motor model block

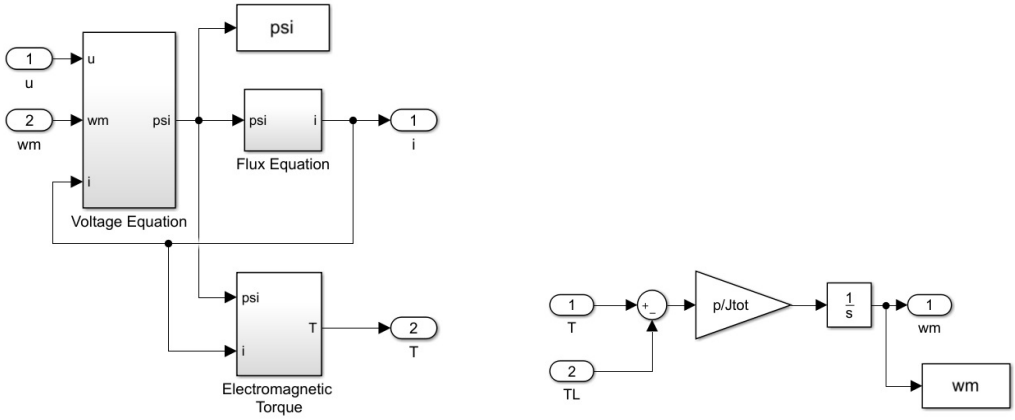

(a) *rotor coordinates block* (b) *mechanics block*

Figure 19: Motor subsystems

In Fig. (a) the relation between flux and current is computed with equations (14), while the voltage equation is (1).

4.2 Pulse Width Modulator and Inverter

With the pulse-width-modulation (PWM) it is possible to generate all the voltages inside of the hexagon, which is shown in Fig. 23. The general principle of the PWM is to compute, for every step, the duty cycle of the switches in order to generate the

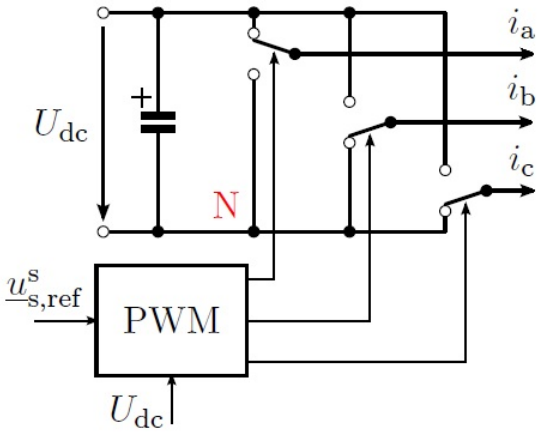

Figure 20: Inverter+PWM scheme

desired voltages and currents. The duty cycle is given by the following relations:

$$\delta_k = \frac{u_{k,ref}}{u_{dc}} + \frac{1}{2} = \frac{T_{k,on}}{T_s} \tag{17}$$

where k is the discrete time index, u_{dc} is the DC-link voltage, $u_{k,ref}$ is the desired voltage, $T_{k,on}$ is the duration of the positive impulse, and T_s is the sample period. For modeling the inverter it is possible to use the schemes in Figures 21 and 22.

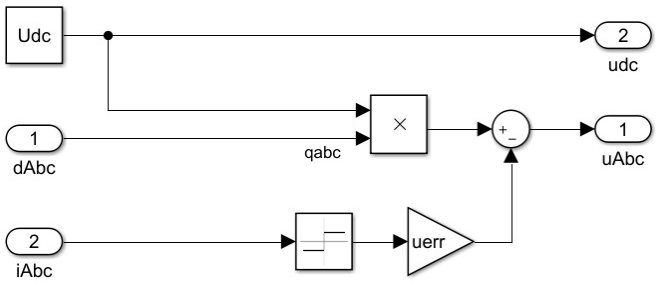

Figure 21: ZOH block

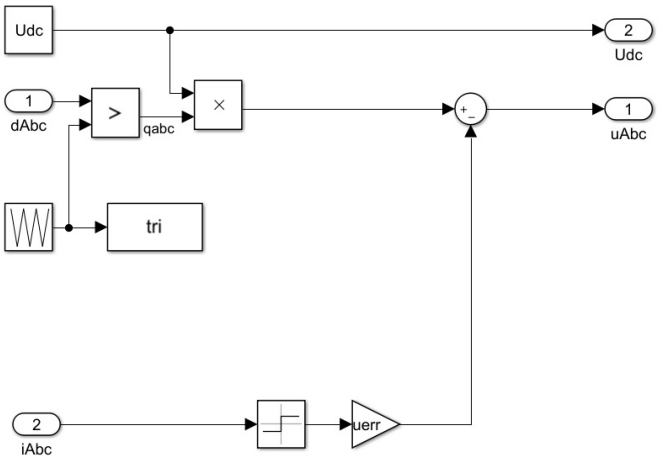

Figure 22: Inverter block

Both the ZOH (Fig. 21) and Inverter (Fig. 22) blocks can be used. The first one multiplies DC-link voltage u_{dc} with the duty cycles of the phases, while in the second one the three duty cycles are compared to a triangle wave, which is varying between 0 and 1

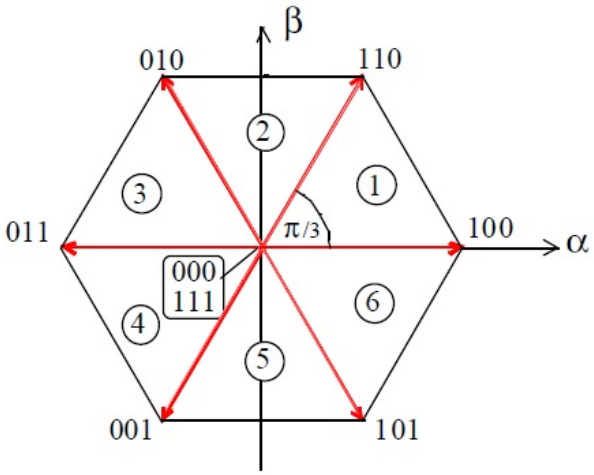

Figure 23: Space Vectors produced by a three-phase inverter

4.3 Current controller

This section is based on [8].

The current controller is composed by a 2DOF (2 degrees of freedom) PI controller, which can be also represented as full-state feedback controllers with integral action and reference feedforward; this framework simplifies the systematic design and analysis of controllers. This type of controller is shown in Fig. 24.

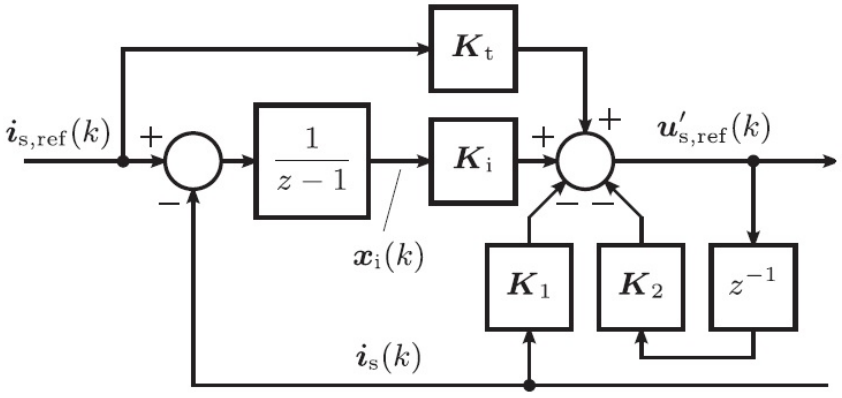

Figure 24: 2 DOF PI controller

The control law is

$$x_\mathrm{i}(k+1) = x_\mathrm{i}(k) + i_{\mathrm{s,ref}}(k) - i_\mathrm{s}(k) \tag{18a}$$
$$u'_{\mathrm{s,ref}}(k) = K_\mathrm{t} i_{\mathrm{s,ref}}(k) + K_\mathrm{i} x_\mathrm{i}(k) - K_1 i_\mathrm{s}(k) - K_2 u_\mathrm{s}(k) \tag{18b}$$

where x_i is the integral state, K_i is the integral gain, K_t is the feedforward gain, K_1 and K_2 are the state-feedback gains, and $u_\mathrm{s}(k+1) = u'_{\mathrm{s,ref}}(k)$.

For digital implementation, continuous-time control control algorithms have to be discretized using Euler method [8].

Continuous-time modeling

In order to model IPMs, real space vectors will be used, for example the stator-current vector is $i_\mathrm{s} = [i_\mathrm{d}, i_\mathrm{q}]^T$, where i_d and i_q are the components of the vector, and the matrix transpose is marked with the subscript T. The identity matrix, the orthogonal rotation matrix, and the zero matrix are respectively defined as

$$\mathbf{I} = \begin{bmatrix} 1 & 0 \\ 0 & 1 \end{bmatrix} \qquad \mathbf{J} = \begin{bmatrix} 0 & -1 \\ 1 & 0 \end{bmatrix} \qquad \mathbf{O} = \begin{bmatrix} 0 & 0 \\ 0 & 0 \end{bmatrix} \tag{19}$$

When the stator-current vector is chosen as a state variable, the state equation becomes

$$\frac{d\boldsymbol{i}_\mathrm{s}(t)}{dt} = \boldsymbol{F}_\mathrm{c}\boldsymbol{i}_\mathrm{s}(t) + \boldsymbol{G}_\mathrm{c}\boldsymbol{u}_\mathrm{s}(t) + \boldsymbol{g}_\mathrm{c}\psi_\mathrm{m} \tag{20}$$

where the inputs are the stator-voltage vector u_s and the PM flux ψ_m, which is constant. The system matrices are

$$\begin{aligned} \boldsymbol{F}_\mathrm{c} &= \begin{bmatrix} -R_\mathrm{s}/L_\mathrm{d} & \omega_\mathrm{m} L_\mathrm{q}/L_\mathrm{d} \\ -\omega_m L_\mathrm{d}/L_\mathrm{q} & -R_\mathrm{s}/L_\mathrm{q} \end{bmatrix} \\ \boldsymbol{G}_\mathrm{c} &= \begin{bmatrix} \frac{1}{L_\mathrm{d}} & 0 \\ 0 & \frac{1}{L_\mathrm{q}} \end{bmatrix} \qquad \boldsymbol{g}_\mathrm{c} = \begin{bmatrix} 0 \\ -\omega_\mathrm{m}/L_\mathrm{q} \end{bmatrix} \end{aligned} \tag{21}$$

where the parameters has been already defined in the previous chapters, and the subscript c refers to the continuous-time model.

Discrete-time modeling

The discrete-time IPM model in rotor coordinates can be expressed as

$$\boldsymbol{i}_\mathrm{s}(k+1) = \boldsymbol{F} i_\mathrm{s}(k) + \boldsymbol{G} u_\mathrm{s}(k) + \boldsymbol{g}\psi_\mathrm{m} \tag{22}$$

where $\boldsymbol{F}$, $\boldsymbol{G}$, and $\boldsymbol{g}$ are the system matrices, and k is the discrete-time index.

The exact system matrices will be computed in the following:

- The matrix $\boldsymbol{F}$ will be expressed using the series expansion

$$\boldsymbol{F} = \mathbf{I} + T_\mathrm{s} \boldsymbol{\Psi} \boldsymbol{F}_\mathrm{c} \tag{23}$$

- The exact input matrix $\boldsymbol{G}$ cannot be easily expressed as a series expansion, however it can be approximated as

$$\boldsymbol{G} \approx T_\mathrm{s} \boldsymbol{\Psi} \boldsymbol{G}_\mathrm{c} \frac{\frac{\omega_\mathrm{m} T_\mathrm{s}}{2}}{\sin\left(\frac{\omega_\mathrm{m} T_\mathrm{s}}{2}\right)} e^{-\frac{\omega_\mathrm{m} T_\mathrm{s}}{2}\mathbf{J}} \tag{24}$$

where T_s is the sampling period and the matrix $\boldsymbol{\Psi}$ is expressed as

$$\boldsymbol{\Psi} = \mathbf{I} + \frac{T_\mathrm{s} \boldsymbol{F}_\mathrm{c}}{2!} + \frac{T_\mathrm{s}^2 \boldsymbol{F}_\mathrm{c}^2}{3!} + \dots \tag{25}$$

Typically, the first two terms of (25) suffice.

For control design, the time delay can be included in the plant model as

$$\begin{bmatrix} \boldsymbol{i}_\mathrm{s}(k+1) \\ \boldsymbol{u}_\mathrm{s}(k+1) \end{bmatrix} = \begin{bmatrix} \boldsymbol{F} & \boldsymbol{G} \\ \mathbf{O} & \mathbf{O} \end{bmatrix} \begin{bmatrix} \boldsymbol{i}_\mathrm{s}(k) \\ \boldsymbol{u}_\mathrm{s}(k) \end{bmatrix} + \begin{bmatrix} \mathbf{O} \\ \mathbf{I} \end{bmatrix} \boldsymbol{u}'_\mathrm{s,ref}(k) + \begin{bmatrix} \boldsymbol{g} \\ 0 \end{bmatrix} \psi_\mathrm{m} \tag{26}$$

where $\boldsymbol{i}_\mathrm{s}$ is the measured feedback, and $\boldsymbol{u}_\mathrm{s}$ is obtained from the previous value of the reference voltage $\boldsymbol{u}'_\mathrm{s,ref}$.

From the previous system, the stator current in the z-domain can be expressed as $\boldsymbol{i}_{\mathrm{s}}(z) = \boldsymbol{Y}(z)\boldsymbol{u}'_{\mathrm{s,ref}}(z)$, where

$$\boldsymbol{Y}(z) = z^{-1}(z\mathbf{I} - \boldsymbol{F})^{-1}\boldsymbol{G} \tag{27}$$

The closed-loop dynamics become

$$\boldsymbol{i}_{\mathrm{s}}(z) = \boldsymbol{H}(z)\boldsymbol{i}_{\mathrm{s,ref}}(z) \tag{28}$$

where

$$\boldsymbol{H}(z) = (z^3\mathbf{I} + z^2\boldsymbol{A}_2 + z\boldsymbol{A}_1 + \boldsymbol{A}_0)^{-1}(z\boldsymbol{B}_1 + \boldsymbol{B}_0) \tag{29}$$

and the coefficient matrices are

$$\begin{aligned}
\boldsymbol{A}_0 &= \boldsymbol{G}(\boldsymbol{K}_2\boldsymbol{G}^{-1}\boldsymbol{F} + \boldsymbol{K}_{\mathrm{i}} - \boldsymbol{K}_1) \\
\boldsymbol{A}_1 &= \boldsymbol{F} + \boldsymbol{G}[\boldsymbol{K}_1 - \boldsymbol{K}_2\boldsymbol{G}^{-1}(\mathbf{I} + \boldsymbol{F})] \\
\boldsymbol{A}_2 &= \boldsymbol{G}\boldsymbol{K}_2\boldsymbol{G}^{-1} - \mathbf{I} - \boldsymbol{F} \\
\boldsymbol{B}_0 &= \boldsymbol{G}(\boldsymbol{K}_{\mathrm{i}} - \boldsymbol{K}_{\mathrm{t}}) \qquad \boldsymbol{B}_1 = \boldsymbol{G}\boldsymbol{K}_{\mathrm{t}}
\end{aligned} \tag{30}$$

The gain matrices can be solved from (30) as

$$\boldsymbol{K}_{\mathrm{t}} = \boldsymbol{G}^{-1}\boldsymbol{B}_1 \qquad \boldsymbol{K}_2 = \mathbf{I} + \boldsymbol{G}^{-1}(\boldsymbol{F} + \boldsymbol{A}_2)\boldsymbol{G} \tag{31}$$

$$\boldsymbol{K}_1 = \boldsymbol{K}_2\boldsymbol{G}^{-1}(\mathbf{I} + \boldsymbol{F}) - \boldsymbol{G}^{-1}(\boldsymbol{F} - \boldsymbol{A}_1) \tag{32}$$

$$\boldsymbol{K}_{\mathrm{i}} = \boldsymbol{K}_1 - \boldsymbol{K}_2\boldsymbol{G}^{-1}\boldsymbol{F} + \boldsymbol{G}^{-1}\boldsymbol{A}_0 \tag{33}$$

Using these expressions, the poles can be arbitrarily placed. The gains depend on the rotor speed via the matrices $\boldsymbol{F}$ and $\boldsymbol{G}$.

Due to the time delay, $\boldsymbol{A}_0 = \mathbf{O}$ is selected and, using a complex vector design, the other coefficient matrices will be

$$\boldsymbol{A}_1 = \beta^2\boldsymbol{F} \qquad \boldsymbol{A}_2 = -\beta(\mathbf{I} + \boldsymbol{F}) \qquad \boldsymbol{B}_1 = (1 - \beta)\mathbf{I} \tag{34}$$

where $\beta = e^{-\alpha T_{\mathrm{s}}}$ is the exact mapping in the discrete time domain of the intended real pole of the system and α is the chosen bandwidth of the current controller.

The Simulink model of the current controller (Fig. 25) is made with a Matlab function block, whose commands have already been described in this section. The system matrices are computed with equations (23) and (24), while L_{d} and L_{q} are kept constant.

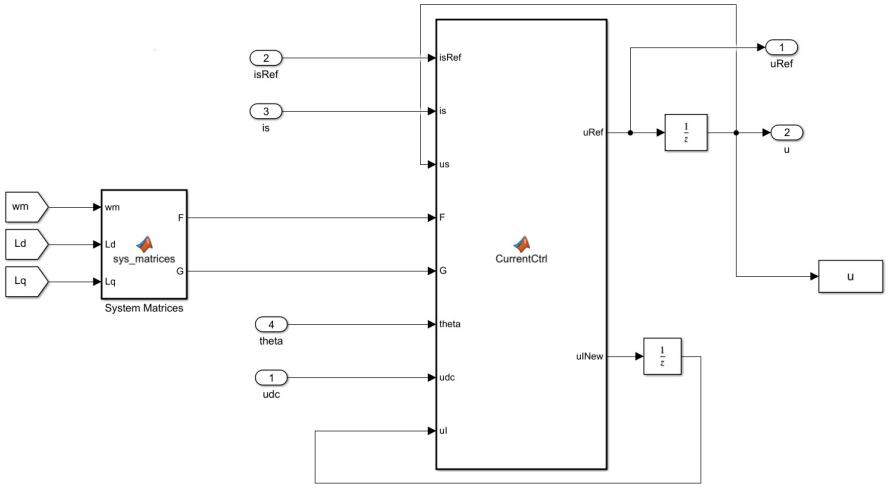

Figure 25: Current controller block

4.4 Flux observer

This section is based on [9].

A flux observer is needed in order to have an exact model of the motor, hence to compute the *dq*-axis inductance, while cross-saturation is acting.

This method will give us a better computation of the system matrices, which are necessary to compute the gain matrices of the current controller.

The equation for this block is

$$\hat{\boldsymbol{\psi}}(k+1) = \boldsymbol{A}\hat{\boldsymbol{\psi}}(k) + \boldsymbol{B}\boldsymbol{u}(k) + \boldsymbol{B}_\mathrm{f}\boldsymbol{\psi}_\mathrm{f} + \boldsymbol{K}_\mathrm{o}[\boldsymbol{L}\boldsymbol{i}_\mathrm{s} + \boldsymbol{\psi}_\mathrm{f} - \hat{\boldsymbol{\psi}}(k)] \tag{35}$$

where the hat stands for the esteemed values, $\boldsymbol{A}$, $\boldsymbol{B}$ and $\boldsymbol{B}_\mathrm{f}$ are the system matrices while the state variable is the flux, $\boldsymbol{K}_\mathrm{o}$ is the observer gain matrix, and k is the discrete-time index.

The continuous-time system matrix with flux as a state variable is represented similarly to $\boldsymbol{F}_\mathrm{c}$ in (21)

$$\boldsymbol{A}_\mathrm{c} = \begin{bmatrix} -R_\mathrm{s}/L_\mathrm{d} & \omega_\mathrm{m} \\ -\omega_\mathrm{m} & -R_\mathrm{s}/L_\mathrm{q} \end{bmatrix} \tag{36}$$

and discrete-time system matrices will be

$$\boldsymbol{A} = \mathbf{I} + T_\mathrm{s}\boldsymbol{\Psi}\boldsymbol{A}_\mathrm{c} \qquad \boldsymbol{B} \approx T_\mathrm{s}\boldsymbol{\Psi}\frac{\frac{\omega_\mathrm{m}T_\mathrm{s}}{2}}{\sin\left(\frac{\omega_\mathrm{m}T_\mathrm{s}}{2}\right)}e^{-\frac{\omega_\mathrm{m}T_\mathrm{s}}{2}\mathbf{J}} \qquad \boldsymbol{B}_\mathrm{f} = T_\mathrm{s}\Psi R_\mathrm{s}\boldsymbol{G}_\mathrm{c} \tag{37}$$

where $\boldsymbol{\Psi} = \mathbf{I} + \frac{T_\mathrm{s}\boldsymbol{A}_\mathrm{c}}{2}$ is expressed as series expansion and $\boldsymbol{G}_\mathrm{c}$ is defined in (21).

It can be seen that the gain matrices are function of the rotor speed ω_m.

4.5 Speed Controller

The speed controller has a similar structure of the current controller, so it is a 2DOF PI controller.

The control law is

$$\begin{aligned} T'_{\text{ref}}(k) &= K_{\text{t}}\omega_{\text{m,ref}}(k) + K_{\text{i}}T_{\text{i}}(k) - K_1\omega_{\text{m}}(k) - K_2T_{\text{ref,lim}}(k) \\ T_{\text{i}}(k+1) &= T_{\text{i}}(k) + \omega_{\text{m,ref}}(k) - \omega_{\text{m}}(k) \end{aligned} \tag{38}$$

where the coefficients are computed with the following relations

$$\begin{aligned} K_{\text{i}} &= \frac{J_{\text{tot}}}{T_{\text{s}}}(\beta-1)^2 & K_1 &= \frac{J_{\text{tot}}}{T_{\text{s}}}(3-4\beta+\beta^2) \\ K_2 &= 2(1-\beta) & K_{\text{t}} &= K_{\text{i}} = \frac{J_{\text{tot}}}{T_{\text{s}}}(1-\beta) \end{aligned} \tag{39}$$

where $\beta = e^{-\alpha_{\text{s}}T_{\text{s}}}$ is the exact mapping in the discrete time domain of the intended real pole of the system and α_{s} is the chosen speed controller bandwidth.

The used Simulink model is shown in figure 26.

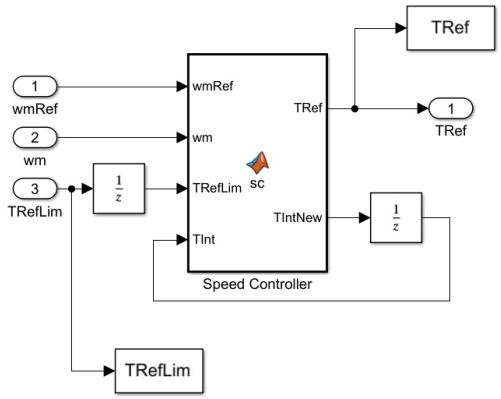

Figure 26: Speed Controller Block

The used matlab function is composed by equations (38) and (39).

4.6 Reference computation block

This section is based on [7].

The reference calculation block aims to compute the reference current value in order to obtain the desired torque, which is computed in the speed controller.

This purpose can be reached through the use of look-up tables, which are a convenient choice due to their efficiency and low computational cost, and through functions.

In the used model, the look-up tables were used, and their computation has been reached thanks to a script provided by Aalto University. The Simulink model is shown below.

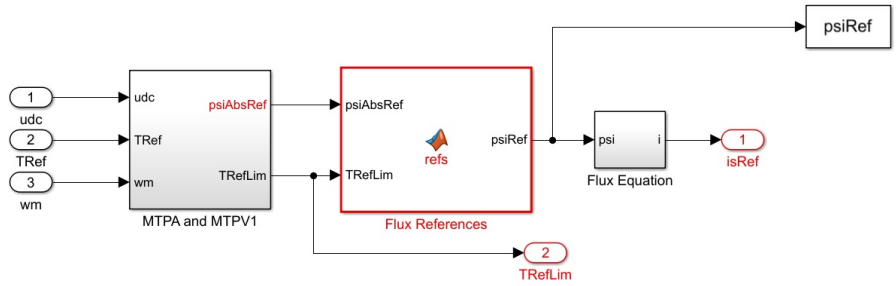

Figure 27: Reference Block

while the MTPA and MTPV block is shown in Fig. 28.

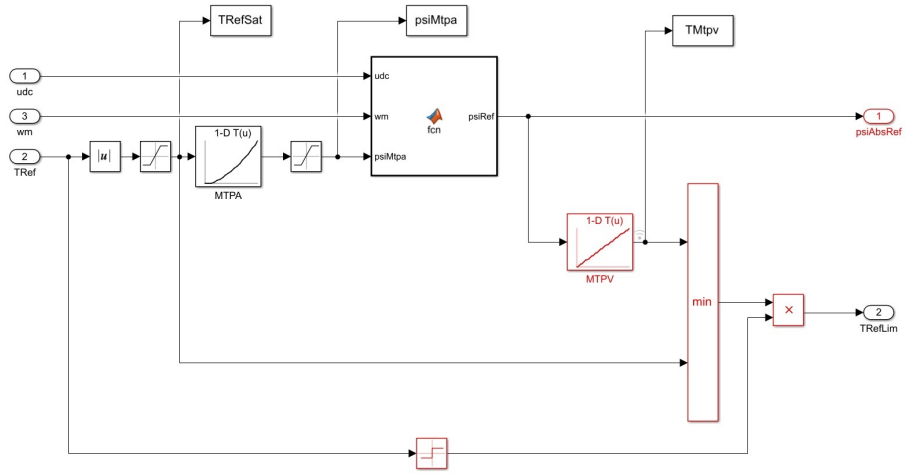

Figure 28: MTPA and MTPV block

Fig. 28 shows how the reference calculation scheme is composed. The optimal MTPA flux magnitude is read from a look-up table, whose input is the torque reference (limited to a fixed torque T_{max}). The MTPA flux is limited based on the maximum available voltage, which is calculated from the measured DC-link voltage u_{dc}.

The flux references block can be explained through the following scheme:

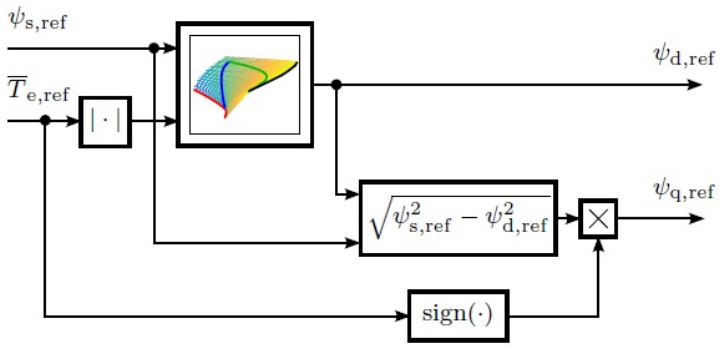

Figure 29: Stator flux reference ([7])

The optimal flux reference is then used to evaluate the current references with equations (14), hence obtaining the outputs i_{d} and i_{q}, which are the inputs of the current controller.

Computation of the Look-up Tables with FEM software

Once we have the MTPA, FW and MTPV loci (Fig. 10), it is easy to compute the required values for the look-up tables from FEM static simulations, which are torque T_{em}, dq fluxes ψ_{dq} and flux amplitude ψ_{s}.

It may be possible that the machine needs to work in the area delimited by the points in Fig. 10. In order to make this possible, the 2D look-up table (Fig. 29) is needed. The inputs are the torque T_{em} and the amplitude of the flux ψ_{s} and the output is the d-axis flux ψ_{d}. The resulting plot of the FEM data is the following

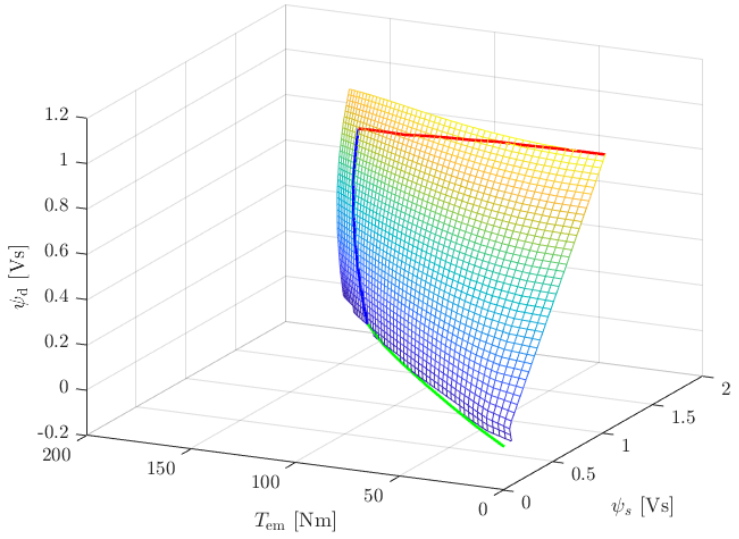

Figure 30: 2D look-up table computed from FEMM

Computation of the Look-up Tables with fixed inductances

In the same manner, once the current loci are computed, it is easy to find the corresponding torque and fluxes values with equations (4) and (3) with fixed values of L_d and L_q.

The 2D look-up table computation leads to the plot shown in Fig. 31.

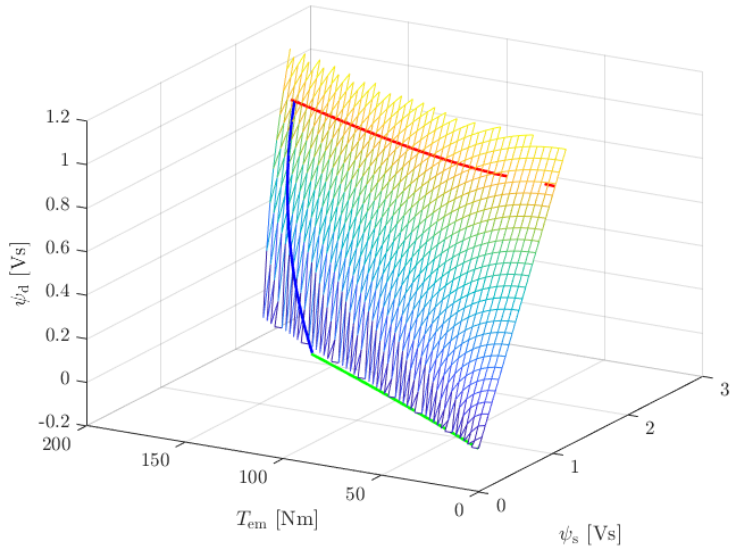

Figure 31: 2D look-up table computed with fixed inductances

It is remarkable even from the computation of the 2D look-up tables that the choice

of L_{d} and L_{q} leads to a similar locus shape.

5 Simulation results

The parameters used for the simulations are listed in Table 9.

Parameter	Value	Description
T_s [s]	$50 \cdot 10^{-6}$	Sampling period of the current control loop
T_{s2} [s]	$50 \cdot 10^{-6}$	Sampling period of the slower subsystem
U_{dc} [V]	1018	DC-link voltage
α_c [rad/s]	$2\pi 500$	Current-control loop bandwidth
α_s [rad/s]	$2\pi 3$	Speed-control loop bandwidth
$k_{u,max}$	0.8	Steady-state voltage margin

Table 9: Used parameters for the simulation

The plots in this section are referred in p.u. to the following base values listed in Table 10.

Parameter	Value
Base voltage [V]	587.87
Base current [A]	5.29
Base speed [rad/s]	314.16
Base torque [Nm]	148.5
Base flux [Vs]	1.87

Table 10: Base values

The simulations are done with two kinds of plant model, one with the linear magnetic model (model 1) and one with the real magnetic model of the motor (model 2), keeping the fixed inductances based parameterization on the control model.

Model	S	T	U	V	a_{d0}	a_{dd}	a_{q0}	a_{qq}	a_{dq}	i_f	ψ_F
1	-	-	-	-	3.046	0	3.001	0	0	3.116	0
2	3	4	0	2	2.683	0.087	3.022	0.018	0.176	3.698	0.220

The types of the simulations depend basically on the given speed reference and the torque load. Every simulation is done with a speed reference equal to 1 p.u. and 3 p.u.

- simulation 1: it aims to show how the system responses to a speed reference step, without a torque load.
- simulation 2: the torque load increases from 0 to T_n with 3 steps every 1 second while the speed reference is kept constant.

- simulation 3: the torque load constantly increases with a rate of $1/3T_{\mathrm{n}}\,\mathrm{Nm/s}$, while the speed reference is kept constant.

5.1 Model 1 - fixed inductances

Here the fixed inductances based plant model is used, hence the motor behaves as expected due to the same parameterization used on the control model.

Simulation 1 (Fig. 32,33)

From the resulting plots, with both speed reference, it can be seen that the raise time is approximately 0.5 s and that the currents and the torque follow the references really good. Furthermore the speed changes slope quite hardly, this is caused probably to the high torque given from the motor and the action of the speed controller.

Simulation 2 (Fig. 34,35)

Figures 34 and 35 show that with speed reference fixed to 1 p.u. the motor can keep that speed satisfying the torque request efficiently, while with speed fixed to 3 p.u. the motor employs some time to reach the desired torque.

Simulation 3 (Fig. 36,37)

In this simulation it can be seen that when T_{load} rises, at a certain point the speed decreases. This happens because, with a constant speed, the motor can give a certain range of torque.

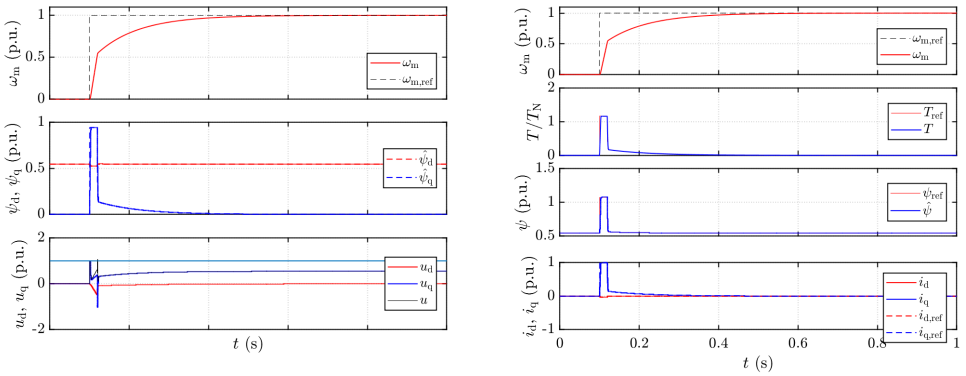

(a) (b)

Figure 32: $\omega_{m,ref} = 1\,\text{p.u.}$

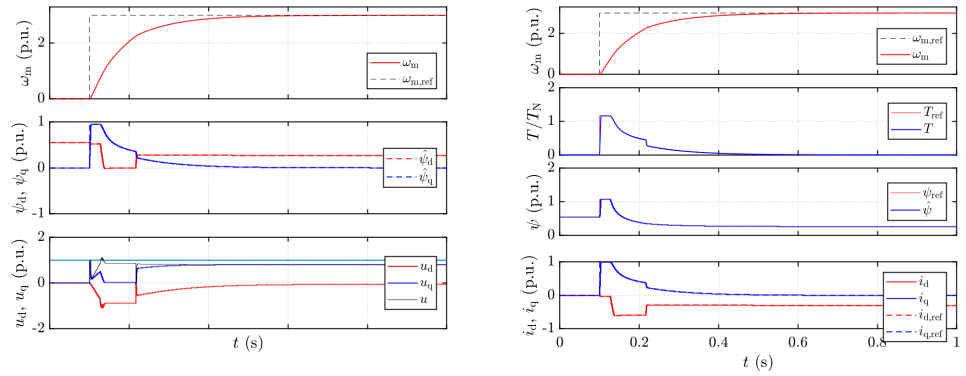

(a) (b)

Figure 33: $\omega_{m,ref} = 3\,\text{p.u.}$

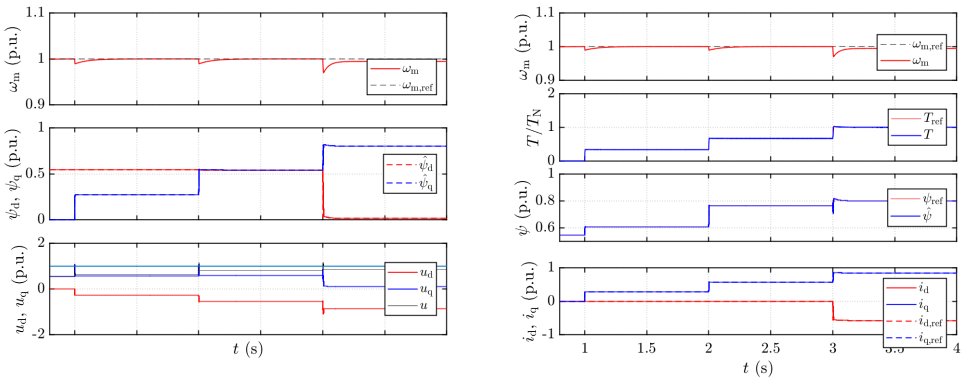

(a) (b)

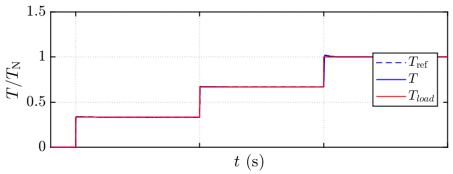

(c)

Figure 34: $\omega_{m,ref} = 1\,\text{p.u.}$

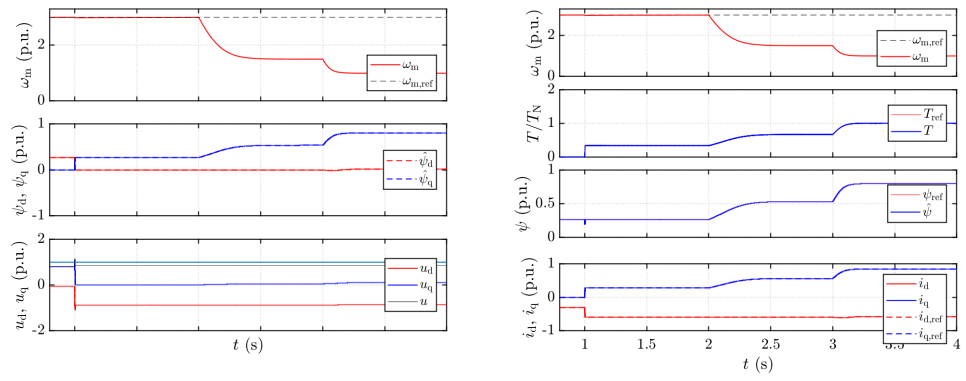

(a) (b)

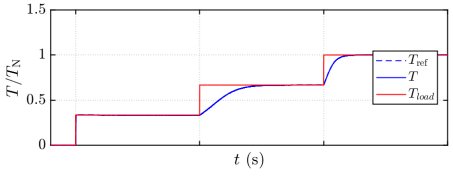

(c)

Figure 35: $\omega_{m,ref} = 3\,\text{p.u.}$

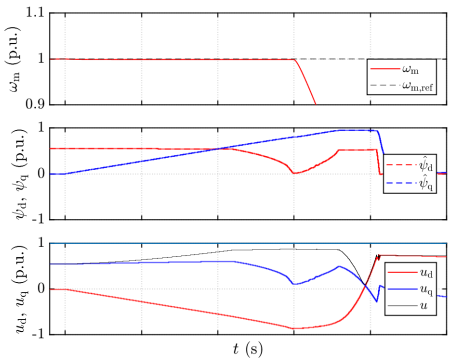

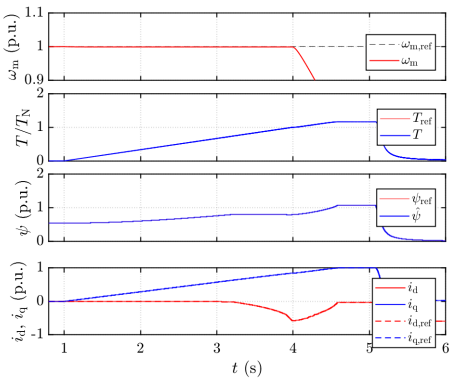

(a) (b)

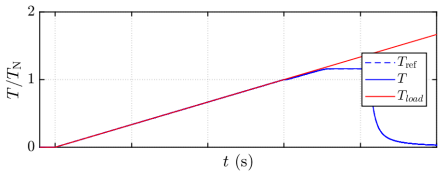

(c)

Figure 36: $\omega_{m,ref} = 1\,\text{p.u.}$

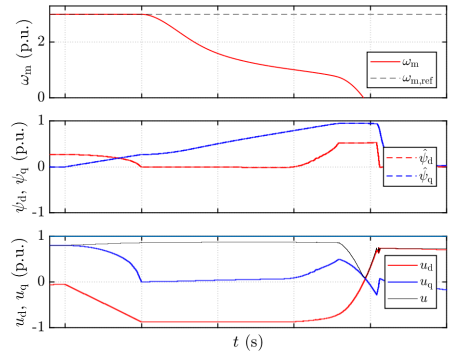

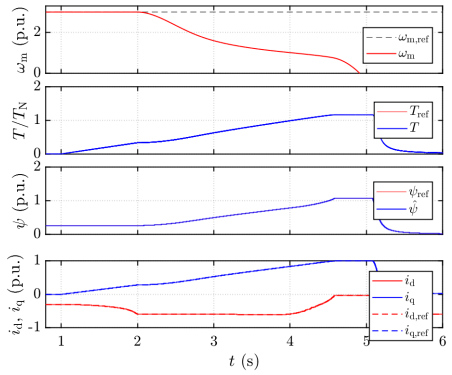

(a) (b)

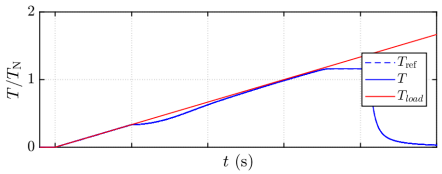

(c)

Figure 37: $\omega_{m,ref} = 3\,\text{p.u.}$

5.2 Model 2 - included cross-coupling and saturation

The following simulations behave a difference between references and given performance of the motor. This happens because there is an error given from the saturation and the cross-coupling. Furthermore the given torque with this model represents the real torque of the motor, in fact it can be seen that the maximum torque given from the motor is less than 1 p.u., this is caused by the error between the real MTPA locus and the fixed inductances based one.

Simulation 1 (Fig. 38,39)

From Figures 38 and 39, it can be seen that, as with the model 1, the raise time is approximately 0.5 s, but the estimated fluxes in the flux observer are different from the real ones due to the non-linearity of the plant model.

Simulation 2 (Fig. 40,41)

In this simulation it can be seen that there's an error between the torque reference and the real torque of the motor, anyway the produced torque satisfies the load torque request. Furthermore with $\omega_{\text{ref}} = 1\,\text{p.u.}$ there is an error also between the speed reference and the electrical speed.

Simulation 3 (Fig. 42,43)

In this simulation, the model 2 behaves in a similar manner as model 1.

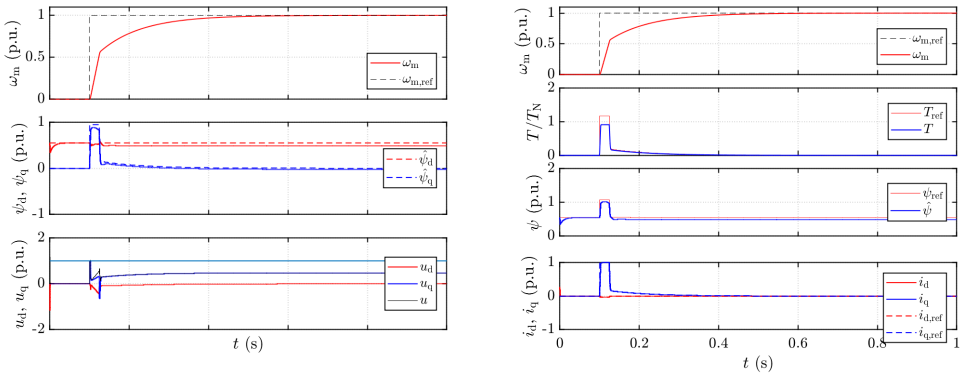

(a) (b)

Figure 38: $\omega_{m,ref} = 1\,\text{p.u.}$

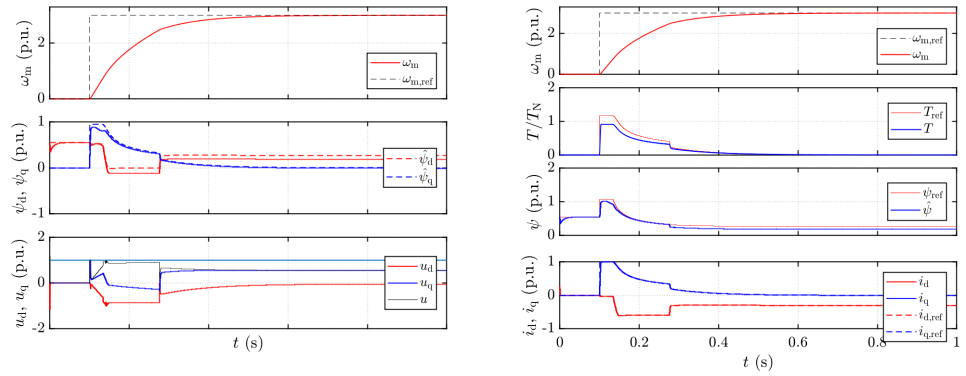

(a) (b)

Figure 39: $\omega_{m,ref} = 3\,\text{p.u.}$

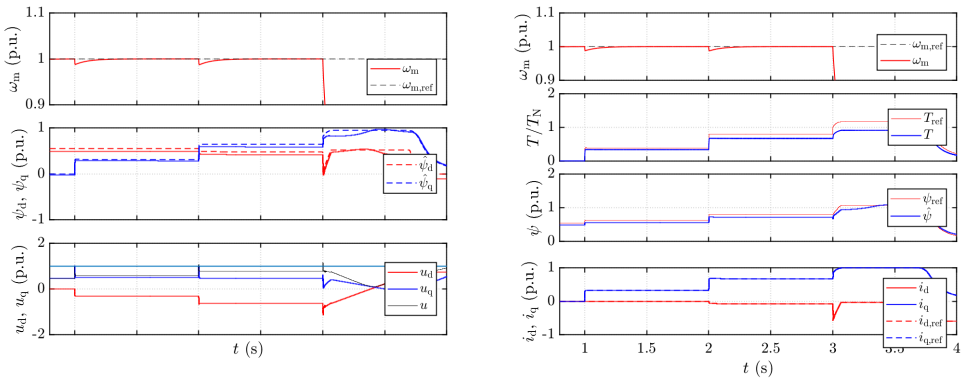

(a) (b)

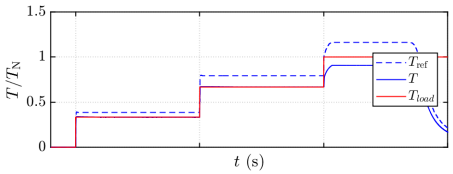

(c)

Figure 40: $\omega_{m,ref} = 1\,\text{p.u.}$

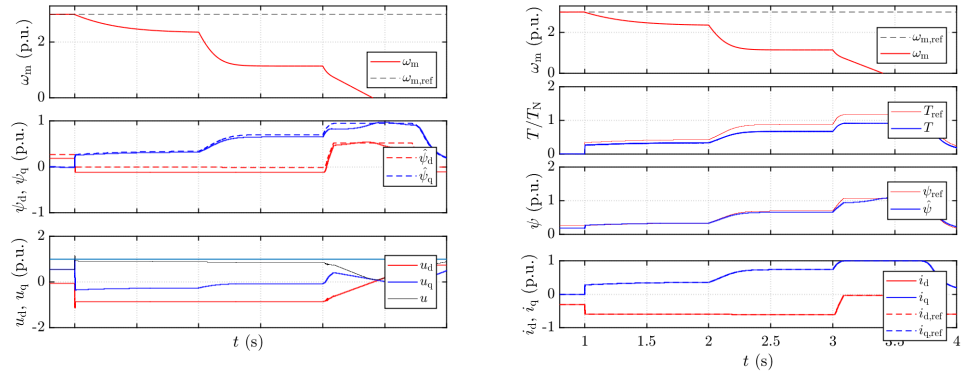

(a) (b)

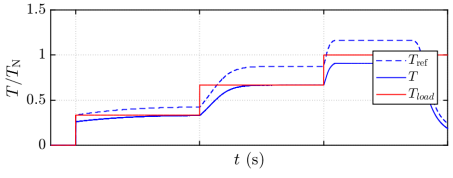

(c)

Figure 41: $\omega_{m,ref} = 3\,\text{p.u.}$

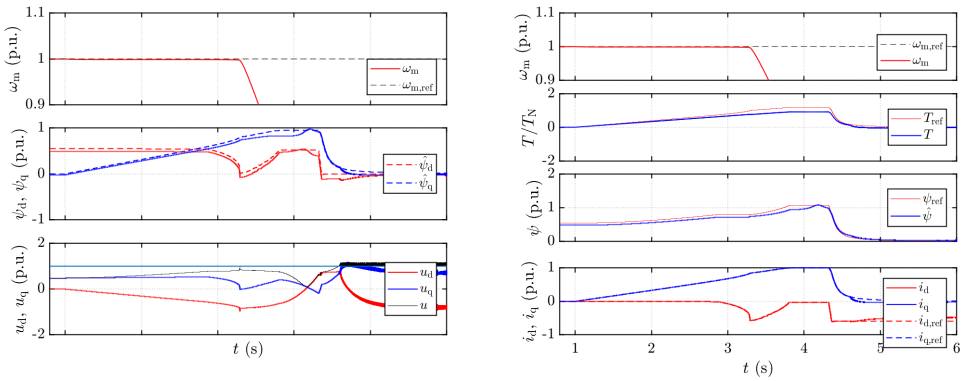

(a) (b)

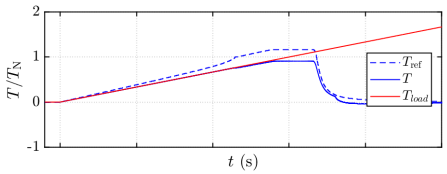

(c)

Figure 42: $\omega_{m,ref} = 1\,\text{p.u.}$

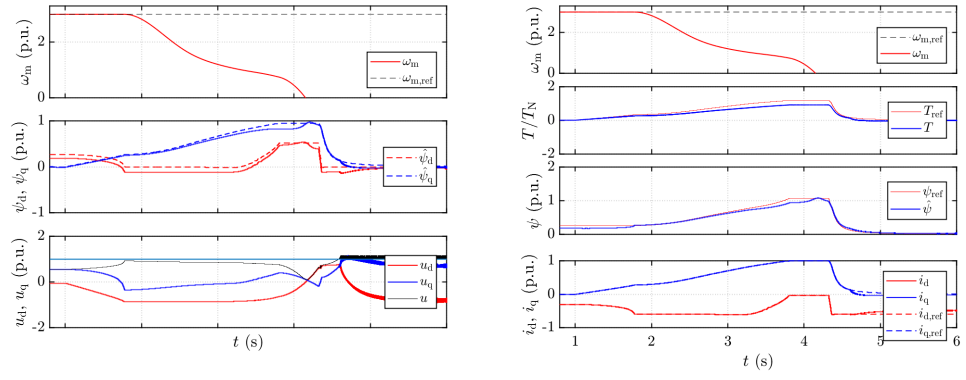

(a) (b)

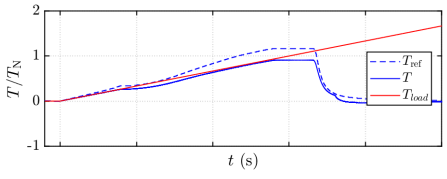

(c)

Figure 43: $\omega_{m,ref} = 3\,\text{p.u.}$

6 Conclusions

In this final project the parameters and the flux maps of the FSPM motor were computed from FEM static simulations. In order to obtain the flux maps, matrices with currents as indices were constructed. Hence these matrices were used to compute the currents as function of the fluxes with the LLS method, which presented an error given from the different equivalent magnetic circuit. This error was decreased with the introduction of an additional parameter leading to a magnetic model similar to the real one computed with FEM.

Then, using these parameters, the MTPA, FW and MTPV operating points were calculated from FEM simulations through some assumptions, which simplified the computation of the loci. After this, a couple of fixed inductances was chosen in order to simplify the control model. The chosen values had to give a similar current locus for the computation of the reference look-up tables.

The chosen control scheme aims to give an optimal torque reference with a low computational cost, thanks to the look-up tables. Then the control model was tested with two kinds of plant models, one with the same parameterization of the control and one with the real characteristics of the FSPM motor. From the simulations emerged that even if the simplified control model gives an error with the saturating plant model, the results are still good enough in order to allow the use of such parameterization. Tests and measurements on the real motor are nevertheless needed in order to confirm these results.

To summarize, the project began with the brief introduction of the FSPM motor. Then the parameters were estimated from FEM simulations, estimated losses and geometry. After this, the operating points were evaluated and a couple of fixed inductances was chosen in order to model the motor and parametrize the control. Then the needed look-up tables for the control scheme were computed both with FEM simulations and with fixed inductances. Finally, the project concludes the simulation results obtained from MATLAB/Simulink environment.

References

[1] E. A. Bellini, *Motore trifase a magneti permanenti switching-flux: Calcolo delle perdite*, thesis of University of Padova, 2016

[2] J. M. Bellini, *Motore trifase a magneti permanenti switching-flux: Ottimizzazione delle prestazioni*, thesis of University of Padova, 2016

[3] S. E. Rauch, L.J. Johnson, *Design principle of flux-switch alternators*, AIEE Trans., vol. 74III - pp. 1261-1268, 1955

[4] Z.Q.Zhu, J. T. Chen, *Advanced Flux Switching Permanent Magnet Brushless Machine*, IEEE Transactions on Magnetics (Volume: 46, Issue: 6), June 2010

[5] E. Hoang, H. B. Ahmed, J. Lucidarme, *Switching flux permanent magnet polyphased synchronous machines*, EPE 97, Trondheim, Norway, September 1997

[6] R. Zeni *Investigation of the sensorless capability of an Induction Motor with intentionally created saliency. Simulations and measurements*, thesis of University of Padova, 2013

[7] H. A. A. Awan, Z. Song, S. E. Saarakkala, M. Hinkkanen, *Optimal torque control of synchronous motor drives: plug-and-play method*, in Proc. IEEE ECCE 2017, Cincinnati, OH, Oct. 2017.

[8] M. Hinkkanen, H. A. A. Awan, Z. Qu, T. Tuovinen, F. Briz, *Current Control for synchronous motor drives: Direct discrete-time pole-placement design*, IEEE Trans. Ind. Appl., vol. 52, no. 2, pp. 1530-1541, Mar./Apr. 2016.

[9] H. A. A. Awan, T. Tuovinen, S. E. Saarakkala, M.Hinkkanen, *Discrete-time observer design for sensorless synchronous motor drives*, IEEE Trans. Ind. Appl., vol. 52, no. 5, pp. 3968-3979, Sept./Oct. 2016.

[10] M. Hinkkanen, P. Pescetto, E. Mölsä, S. E. Saarakkala, G. Pellegrino, R. Bojoi, *Sensorless self-commissioning of synchronous reluctance motors at standstill without rotor locking*, IEEE Trans. Ind. Appl., vol. 53, no. 3, pp. 2120-2129, May/June 2017.

[11] Huitao Li, Guangkun Lian, Biao Chen, Guobiao Gu, *Vector Control for Flux-Switching Permanent Magnet Machine Based on SVPWM*, IEEE, 2017

[12] N. Bianchi, Christian Babetto, *FERAL, Finite Element Rapid Analysis Lab*, EDLab Padova, sourceforge.net, October 16, 2017

[13] Guangkun Lian, Fuchuan Song, Biao Chen, *Sensorless Control for Flux-Switching Permanent Magnet Machine Based on Sliding Mode Observer*, IEEE, 20th International Conference on Electrical Machines and Systems (ICEMS), August 2017